

Air Curtain Design for Attenuation of Air Gun Signals

December 2008

**Consultant Report to
Stress Engineering Services, Inc.
Houston, TX**

This report has been prepared in confidence for Stress Engineering Services, Inc. No part of this report should be taken in isolation or out of context and interpreted in a manner inconsistent with the overall framework and intent of this document.

by

Warren T. Jones, Ph.D., P.E. (Inactive)

**6202 N. Woods Ln
Katy, TX 77494**

**Tel: 281-391-2398
wjones984@comcast.net**

TABLE OF CONTENTS

	Page
ABSTRACT	ii
INTRODUCTION.....	1
CONCLUSIONS AND RECOMMENDATIONS.....	3
Conclusions	3
Recommendations	3
AIR CURTAIN DESIGN	4
Characteristics of an Air Bubble Curtain.....	4
Bubble Size	5
Gaps in Curtain of Bubbles	5
Speed of Sound and Specific Impedance in the Air-Water Mixture	6
Nozzle-Manifold Geometry and Flow Rates	7
Plume Equations.....	8
Lagrangian Analysis	9
Governing Equations.....	9
Non-dimensionalization.....	10
Relationship of Top Hat and Actual Velocity Profiles	13
Specific Momentum Flux and Characteristic Length of Buoyant Jet Flow	14
Compressible Fluid Flow Through the Nozzles	15
Manifold Design	16
Calculation of Manifold Length	18
OPTIMAL DESIGN.....	20
Principles	20
Application to Air Curtain Design.....	20
RESULTS.....	22
Selection of a “Best” Design	22
Discussion of Selected System	25
REFERENCES.....	28
APPENDICES	
A – Compressibility of Air	
B – Isolated Bubble Trajectory	
C – Excel Workbook Air Curtain Design.xls	
D – Comparison with Experiments	
E – Solution Matrix	

ABSTRACT

A study of methods and equipment for reducing lateral noise propagation from seismic exploration vessels indicated that an air bubble curtain represents a relatively simple system of attenuating seismic signals. In order to further evaluate such a system, it is necessary to determine sizes of manifolds and nozzles, manifold pressure, air volume flow rates, and how to locate manifolds with respect to the seismic air gun arrays.

Equations describing the flow of air in a rising plume of air bubbles, the flow of air through nozzles, and design of a pressure distributing manifold are combined into an optimization problem which minimizes the pneumatic horsepower required to produce a selected value of the speed of sound in the plume of air bubbles. Selecting different values for number and size of nozzles, depth, and maximum speed of sound in the plume produces a different optimal solution for size of manifold, air pressure, and volume flow rate. So a matrix of solutions is generated. Without going into a detail design, the "best" solution is a matter of engineering judgment.

The selected system has a 9-inch manifold towed at a depth of 60 feet below the surface. The manifold has 1/8 inch nozzles spaced 4 inches apart. Pneumatic horsepower and volume flow rate are 423 hp and 4933 scfm, respectively. The manifold is 201 feet long and should be towed 141 feet in front of the air gun array.

Air Curtain Design for Attenuation of Air Gun Signals

by

Warren T. Jones, Ph.D., P.E.(Inactive)

INTRODUCTION

Stress Engineering Services, Inc. is conducting a study of methods and equipment for reducing lateral noise propagation from seismic exploration vessels operating in the Alaskan Beaufort and Chukchi Seas [Ayers (2007)]. Early results of this study, including Spence (2008), indicated that an air curtain represents a relative simple system of providing attenuation of seismic signals. A sketch of the system under consideration is shown in Figure 1.

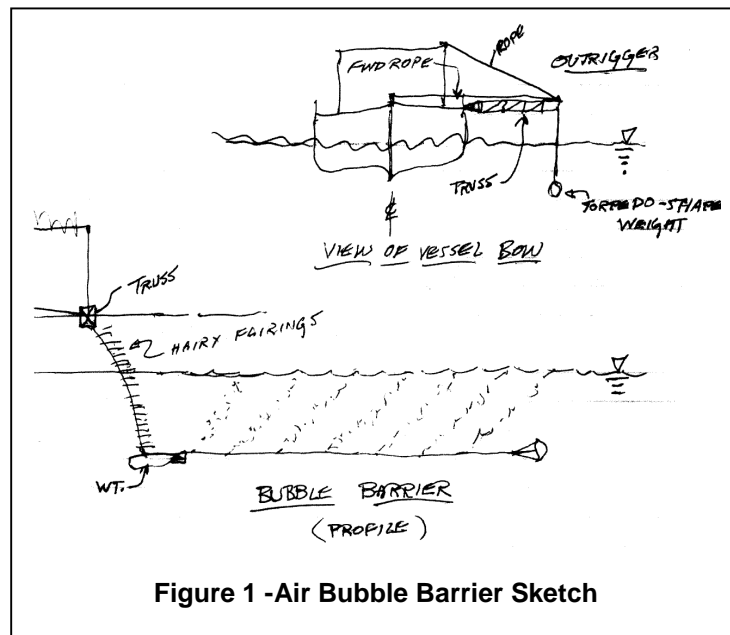


Figure 1 - Air Bubble Barrier Sketch

In order to proceed from a sketch to a design, several questions were posed as the basis for the present investigation [documented in Jones (2008)].

- What is the expected bubble diameter and plume shape; and what is the variation in diameter and shape with water depth
- How should the air be introduced into the water column in order to create a bubble curtain in the correct location with respect to the air gun array? That is, should the manifold be horizontal, or vertical, or both? What is the length of the manifold and its position with respect to the ship and the air gun array?
- Will holes occur in the bubble curtain? If so, how can they be prevented?
- What size should the manifolds be and what air flow rate and pressure is necessary?
- What is the equivalent acoustic impedance of the bubble curtain? This will allow selection of a material for proof-of-concept testing without the necessity of building a complete air curtain system.?

In other words, the objective of this project is to develop a feasibility design of a towed, air bubble barrier. Although the ultimate feasibility will be determined by the acoustic properties of the bubble barrier, no acoustic investigation is included here.

The next section of this report contains the Conclusions and Recommendations resulting from this study. The following section describes the equations used in answering the above equations. Following this is a short section describing the principles of Optimal Design and their application to design of air curtains. The last section presents and discusses the results of this study and the selection of a “best” design.

CONCLUSIONS AND RECOMMENDATIONS

Conclusions

An air bubble curtain is developed by forcing air from a manifold through nozzles. The air exits as a buoyant jet into the sea water, but within a short distance, the jet momentum is dissipated, and further motion is controlled by buoyancy. The rising stream of air is broken into bubbles by the turbulence caused by introducing the jet of air into the water. As a result of the balance between bubble breakup caused by the turbulence and bubble coalescence, all of the bubbles are about 1/4" inch in diameter. This phenomenal fact means that studies of individual bubbles rising in a column of water do not apply to the design of an air bubble curtain.

The only gaps in the air bubble curtain will occur near the manifold where the air from one nozzle has not yet merged with air from the adjacent nozzle. For nozzles spaced 3 or 4 inches apart, there will be a triangular gap with a height of 12 or 16 inches above the manifold. This gap is relatively small and will actually contain a small amount of air, so it is considered insignificant.

Equations developed for a two-dimensional, or line, plume previously have been found to apply to a buoyant flow exiting from a series of nozzles in a manifold into an ambient fluid. Here, "plume" means fluid motions produced by a continuous source of buoyancy. As the air rises, it entrains water into the flow, so the volume fraction of air in the plume decreases. But as the air rises, the pressure is reduced, and the volume of the air increases. As a result of these two opposing effects, the speed of sound and the specific acoustic impedance in the plume vary with height above the manifold.

The governing equations for a two dimensional plume have been combined with the equations for the compressible flow of air through a nozzle and the equations for the design of a pressure distribution manifold to create an optimization problem. By minimizing the pneumatic horsepower in the manifold (pressure times flow rate), an optimum solution is obtained based on specified configurations and constraints. Changing nozzle diameter, number of nozzles per ft along the manifold, or the manifold depth will produce a different optimal solution. In this way a matrix of solutions for different manifold depths below the surface was generated. Selection of a "best" design out of this matrix of solutions is based on engineering judgment.

The recommended "best" design is shown as Solution #58 in Table E - 2 of Appendix E and discussed under the heading "Discussion of Selected System" on page 25. The manifold for this system is located 60 ft below the surface. It has a diameter of 9", a length of 201 ft, and 3 – 1/8 inch nozzles per ft. The maximum ratio of speed of sound in the air curtain to speed of sound in water of 0.07 is obtained with 423 hp and a flow rate of 4933 scfm.

Recommendations

Previous tests on air bubble barriers in the literature have concentrated on measuring signals and their attenuation with little attention to what was generating the air bubble barrier. Therefore, it is recommended that experimental measurements made during a Proof-of-Concept test include measurements of all variables pertaining to the air flow as well as those pertaining to attenuation of seismic signals.

Although not considered in this report, an air bubble barrier generates noise of its own. It is recommended that further investigation be conducted to determine the effect of air bubble barrier noise on marine life that the barrier is meant to protect.

The present analysis neglects the effect of a free water surface. Near the surface, water is no longer entrained into the rising plume. In this region, water falling from the mound created above the water surface meets the rising air-water mixture. The result is a horizontal current at the surface moving away from the plume centerline, so entrainment cannot occur. If the speed of sound in the plume near the surface turns out to be critical for sufficient attenuation of the seismic signal, a more detailed analysis of the plume in this region will be necessary.

AIR CURTAIN DESIGN

An air bubble curtain is developed by forcing air through orifices, or nozzles, in a manifold. Let the manifold be aligned with the x -axis of a coordinate system as shown in Figure 2. The manifold (and x -axis) are located at a depth, H , below the water surface. The z -axis is pointed upward, and measures height above the nozzle exit. The y -axis is oriented to form a right-hand coordinate system.

Several assumptions will be made in order to simplify the following analysis as much as practical. First, the ocean is assumed to be of uniform density. The following equations can be adapted to a stratified ocean or to an ocean with continuously varying density. However, for this first feasibility analysis, the ocean density and temperature are assumed to be constant.

Another simplifying assumption is that the air traveling from the ship to the manifold and along the manifold is at the temperature of the sea water. If the manifold is far enough away from the air compressor, the air could well be approaching the sea water temperature. But it could also be different. Accounting for actual air temperature at the entrance to the manifold will await a detailed, final design analysis.

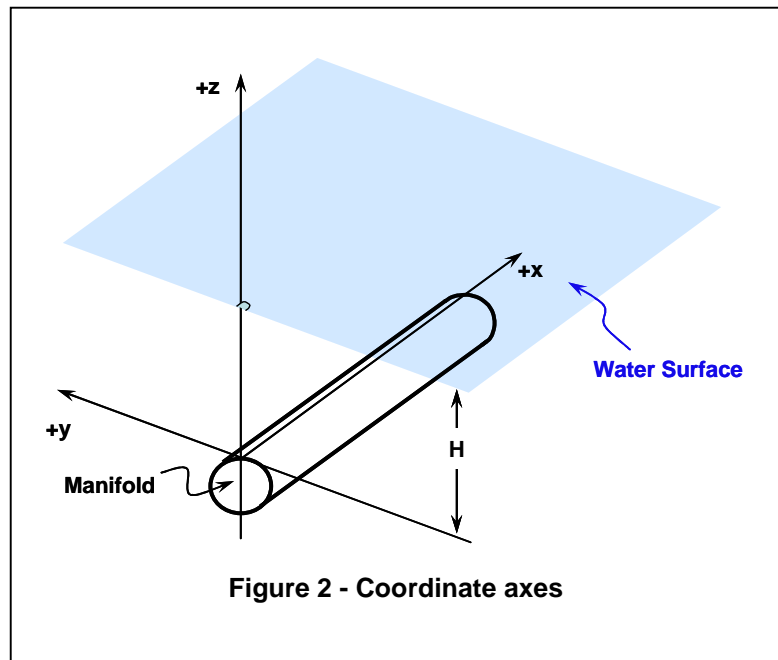


Figure 2 - Coordinate axes

Characteristics of an Air Bubble Curtain

Circulation patterns in the water and velocity profiles in and around an air bubble curtain are shown in Figure 3. This is a view looking along the manifold in the positive x direction. As the bubbles rise, they entrain water, and the vertical average velocity profile of the air-water mixture is well represented by a Gaussian profile, as shown. The air in the mound of air-water mixture at the surface escapes into the atmosphere, and the water runs downhill, creating a surface velocity as shown on the right side of the figure. The magnitude of this velocity is important when an air bubble curtain is used as a breakwater, or to contain an oil spill. However, for the purpose of attenuating air gun signals, the volume fraction of the air in the rising plume is the most important characteristic.

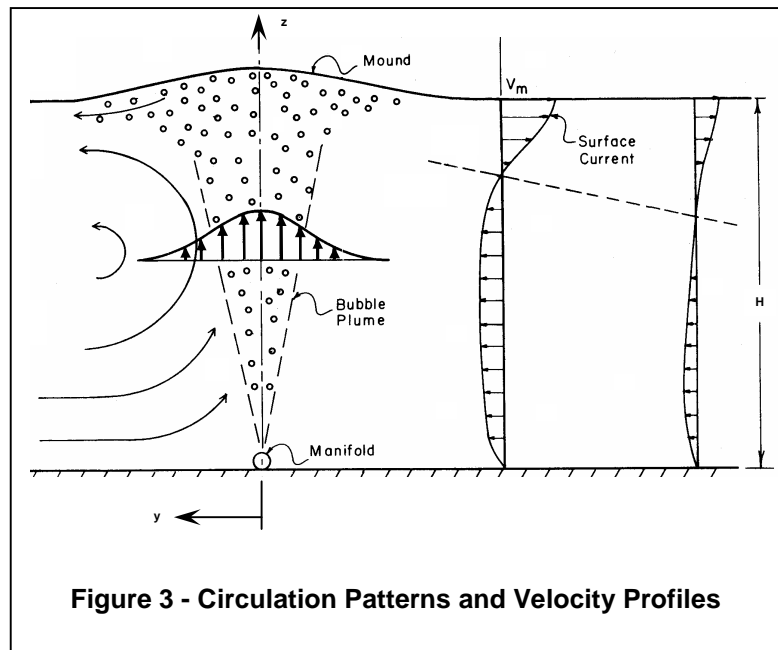


Figure 3 - Circulation Patterns and Velocity Profiles

Bubble Size

Jones (1972) conducted large scale experiments on an air bubble curtain in 7 ft of water in the 6-ft wide test section of a current tank. Based on observations (not measurements) in still water, the majority of the air bubbles in the rising plume were on the order of $\frac{1}{4}$ inch in diameter. Only a comparatively few bubbles were larger – on the order of $\frac{3}{4}$ - to 1-inch.

The explanation for this is found in the work done by Towell, Strand et al. (1965) on sparged towers. They observed that when air was introduced through a sparger (a nozzle containing multiple orifices) at the bottom of a column of water in a Plexiglas tube, the air bubbles were all approximately $\frac{1}{4}$ -inch in diameter no matter what type of sparger was used or what size orifices were in the sparger. The bubble size remained constant over the entire 10-foot height of the water column. This is in direct contradiction to the notion that a bubble of gas should expand as it rises in a column of liquid. High speed photography was used to explain this paradox. Individual bubbles were observed during the process of coalescing with other bubbles and breaking up. The fact that the size was independent of elevation is explained by a balance between breakup and coalescence. Small bubbles touch and coalesce until a bubble size is reached that is unstable in the turbulence created by the rising bubble plume. The intensity of turbulence in the center of the plume depends only on the flow rate of the air, so it is approximately the same at all elevations.

Towell, Strand et al. (1965) found the bubble size to be independent of air flow rate, and explained this as follows. The higher air flow rates result in higher coalescence rates, but the intensity of turbulence is also higher, resulting in a higher rate of breakup. This balances the increased coalescence rate and keeps the bubble size constant.

This explanation agrees with all the observations made during the air barrier tests of Jones (1972); no matter what the air flow rate was, the bubble size was always about the same. The only exception occurred at very low air flow rates where the bubbles were not close enough to coalesce or create much turbulence. This constant bubble size explains why previous investigations of the use of air barriers as breakwaters found no effect of orifice size on the surface current produced.

Gaps in Curtain of Bubbles

At air flow rates commonly used in air curtains, the bubbles are continually coalescing and breaking up. So the bubbles remain in close proximity to each other at all times. Visual observation in the tests of Jones (1972) confirmed that there were no gaps, or holes, in the curtain of bubbles.

However, near the manifold, there will be gaps between nozzles where the air from one nozzle has not yet merged with air from the adjacent nozzle. Both the width and height of this gap will depend on the nozzle spacing.

Consider a series of nozzles discharging air into the water as shown in Figure 4. The nozzles have a circular exit and are spaced a distance L_N apart. Above a certain height, the circular jets of air merge, and from there to the surface, the effect is that of a two-dimensional, or line plume. [See “Plume Equations” on page 8.]

The rate of spreading for a circular buoyant jet may be used to calculate the height, h , where air from adjacent nozzles merge. From dimensional analysis and experiments, Lee and Chu (2003) give the half-width of a jet as

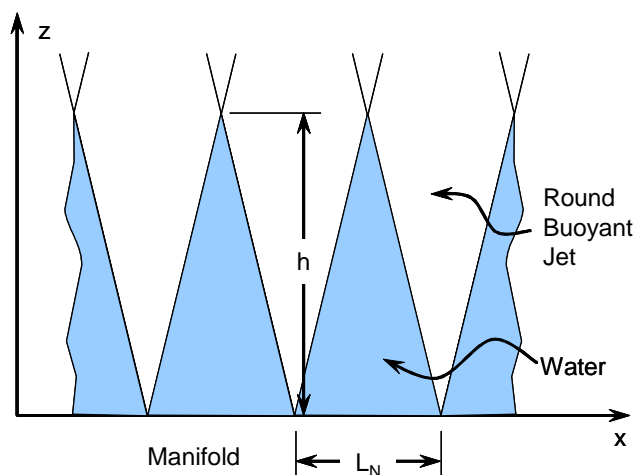


Figure 4 – Gaps in the Bubble Curtain at the Manifold

$$b\lambda = 1.19(0.105)z = 0.125z \quad (1)$$

where b is the half-width of the Gaussian velocity profile, and λ is a factor to account for the air spreading faster than the average velocity spreads. Setting $b\lambda$ equal to one-half the distance between nozzles, L_N , allows the distance h to be calculated as

$$h = 4L_N \quad (2)$$

So there is a triangle of water with base L_N and height $4L_N$ between nozzles. However, it is not pure water; there is some air in it. The width of a Gaussian profile extends from $-\infty$ to $+\infty$. The half-width b of the Gaussian velocity profile is the distance from the centerline to where the velocity is $1/e$ times the centerline velocity. So there will be some air in this triangle between nozzles.

For nozzles space 3 or 4 inches apart, the height h is 12 or 16 inches. Allowing for the fact that there will be some air in this triangle, the effect of this gap on the overall performance of the air curtain is insignificant.

Speed of Sound and Specific Impedance in the Air-Water Mixture

Attenuation of an air gun signal traveling through an air bubble curtain occurs because the speed of sound in the curtain is less than the speed of sound in sea water. Therefore, to begin an investigation of air curtain design, it is necessary to define the speed of sound in the air bubble curtain.

In general, the speed of sound, c , in any kind of material is given by

$$c = \sqrt{\frac{g}{\beta\rho}} \quad (3)$$

where g is the acceleration of gravity, β is the compressibility of the material, and ρ is the density of the material.

Domenico (1982) gives the following equations for compressibility and density of an air-water mixture

$$\begin{aligned} \beta &= (1-s)\beta_w + s\beta_a \\ \rho &= (1-s)\rho_w + s\rho_a \end{aligned} \quad (4)$$

where the subscripts w and a refer to water and air, respectively, and s is the volume fraction of air in the flow. The result of substituting Equations (4) into Equation (3) is the same as Equation (3) of Costigan and Whalley (1997) which matched their experimental results.

The density and compressibility of water are taken as constants. The density of air is given by the perfect gas relationship

$$P = \rho_a RT \quad (5)$$

where P is the pressure, T is the temperature in $^{\circ}\text{R}$, and R is the gas constant for air = 53.36 ft-lb_f/lb_m- $^{\circ}\text{R}$. The compressibility of air is given by [see Appendix A]

$$\beta_a = \frac{1}{P} \quad (6)$$

If Q_a is the volume flow rate of air and Q is the volume flow rate of the air water mixture, then

$$s = \frac{Q_a}{Q} \quad (7)$$

Substituting Equation (4) into Equation (3) gives the speed of sound in the air curtain. Using the values of β_w and ρ_w for water and $s = 0$ gives the speed of sound in water, c_w . In the following, the ratio of c to c_w will be used as a measurement of the efficiency of the air barrier curtain.

$$\frac{c}{c_w} = \sqrt{\frac{\beta_w \rho_w}{[(1-s)\beta_w + s\beta_a][(1-s)\rho_w + s\rho_a]}} \quad (8)$$

Specific Impedance I is defined as

$$I = c\rho$$

Using Equations (3) and (4), the specific impedance for the air curtain can be written as

$$I = \sqrt{\frac{(1-s)\rho_w + s\rho_a}{(1-s)\beta_w + s\beta_a}} \quad (9)$$

Using the values of β_w and ρ_w for water and $s = 0$ gives the specific impedance of the sea water I_w , and the ratio I/I_w is given by

$$\frac{I}{I_w} = \sqrt{\frac{\beta_w (1-s)\rho_w + s\rho_a}{\rho_w (1-s)\beta_w + s\beta_a}} \quad (10)$$

Nozzle-Manifold Geometry and Flow Rates

Before delving into the fluid mechanics of the rising air-water mixture in the bubble plume, a few definitions are in order. Let

- n = Number of nozzles per unit length
- q_o = Volume flow rate through a single nozzle
- Q_o = Volume flow rate per unit length
- m_o = Mass flow rate through a single nozzle
- m_a = Mass flow rate of air per unit length

Then

$$\begin{aligned} Q_o &= n q_o \\ m_a &= n m_o \end{aligned} \quad (11)$$

The spacing of the nozzles, L_N , is given by

$$L_N = \frac{1}{n} \quad (12)$$

Let

Q_{oT} = Total flow rate into manifold

L_M = Length of manifold

Then

$$Q_{oT} = nq_o L_M = Q_o L_M \quad (13)$$

It should be noted that Q_{oT} is the total volume flow rate into the manifold at the pressure, P , and temperature, T , of the air. The volume flow rate at standard conditions is given by

$$Q_{oT} \text{ in scfm} = Q_{oT} \frac{P}{P_{std}} \frac{T_{std}}{T} \quad (14)$$

where "scfm" is standard cubic feet per minute and Q_{oT} is expressed in cubic feet per minute. The usual definition of "standard conditions" is atmospheric pressure and a temperature of 68 °F = 527.69 °R..

Plume Equations

Jones (1972) found that previous investigators used equations developed for a two-dimensional, or line, "plume" to describe an air bubble curtain used as a breakwater. Here, "plume" means fluid motions produced by continuous sources of buoyancy - for example, the hot air rising over a forest fire. Since 1972 more investigations, both theoretical and experimental, of the fluid mechanics of buoyancy-driven flows have been accomplished. An excellent source for the results of these investigations is the book by Lee and Chu (2003).

Even though air is exhausted through individual nozzles spaced a distance L_N apart, the majority of the air bubble curtain can be treated as the two-dimensional plume above a line source of buoyancy. The large scale experiments of Jones (1972) confirmed the applicability of the 2-D plume equations to the generation of a horizontal surface current by an air bubble curtain. Lee and Chu (2003) also take this approach in analyzing the dilution of effluent from ocean outfalls consisting of nozzles spaced along a manifold. Unfortunately, their analyses are all for effluents having a constant density which is very close to that of water. Fortunately, their formulation is directly applicable to an "effluent" of air having a density which varies with height above the manifold and which is greatly different from that of water.

A 2-D plume can be generated by discharging air through a continuous slot in the top of a manifold. The equivalent slot width, $2B_o$, which discharges the same mass and volume of air per unit length as n nozzles per unit length of diameter d is

$$2B_o = n \frac{\pi d^2}{4} \quad (15)$$

Lagrangian Analysis

The velocity profile in a rising plume has a Gaussian distribution as indicated in Figure 3. However, analysis of the air-water mixture in the plume is considerably simplified by the use of a “top-hat” profile

$$\begin{aligned} w &= W \text{ if } |y| \leq B \\ &= 0 \text{ otherwise} \end{aligned} \quad (16)$$

where W and B are the velocity and half-width of an equivalent jet with a sharp boundary and uniform velocity, W , carrying the same mass flow and momentum flux as the actual plume.

Consider the Lagrangian plume element indicated in Figure 5. As it exits from the nozzle, it has a velocity W_o , a half-width B_o , and a length in the z -direction of $W_o\Delta t$, where Δt is a small time increment. At time t , it has risen to a height z above the nozzle, and it has a velocity W , a half-width B , and a length in the z -direction of $W\Delta t$.

Governing Equations

Because this is a Lagrangian formulation,

$$\frac{dz}{dt} = W \quad (17)$$

Conservation of mass per unit length of manifold requires that

$$\begin{aligned} Q &= Q_a + Q_w \\ m &= m_a + m_w \\ m_a &= \text{const} \end{aligned} \quad (18)$$

where subscript “a” refers to the air, subscript “w” refers to the water, and no subscript indicates the mixture. In general, mass flow rate $m = \rho Q$. Conservation of momentum flux, M , requires

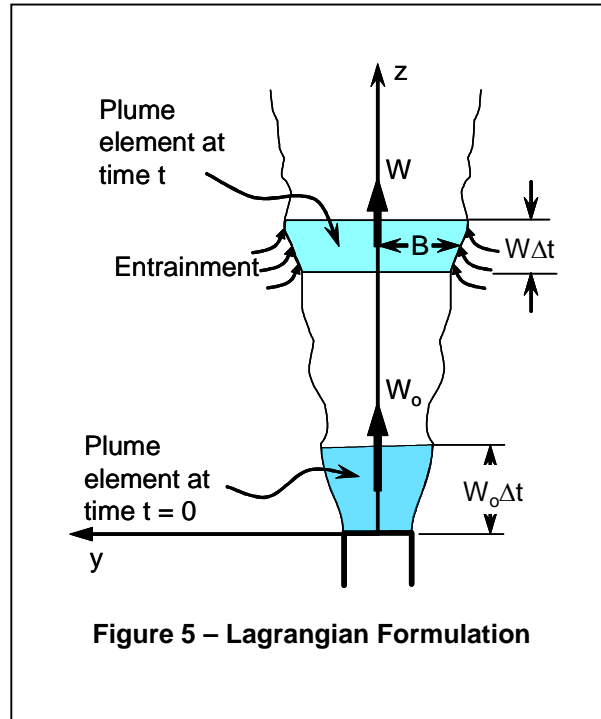
$$\frac{dM}{dt} \equiv \frac{d}{dt}(\rho Q W) = F \equiv (\rho_w - \rho_a)gQ \quad (19)$$

where F is the buoyancy flux.

The entrainment hypothesis is used to provide for turbulent closure. The entrained volume flux, Q_e , is taken to be proportional to the velocity W so that

$$Q_e = \alpha W \Delta z$$

where α is the coefficient of entrainment. Because the entrained fluid consists entirely of water



$$dQ_w = Q_e = \alpha W \Delta z = \alpha W^2 \Delta t$$

where the second equality is a result of Equation (17). Dividing by Δz and Δt and taking the limit gives

$$\frac{dQ_w}{dz} = \alpha W \quad \text{or} \quad \frac{dQ_w}{dt} = \alpha W^2 \quad (20)$$

Because flow in the plume is a boundary layer flow, the pressure is constant in the y -direction. Since air is treated as a perfect gas, the density of the air is given by

$$\rho_a = \frac{P}{RT} = \frac{\rho_w(H - z) + P_{atm}}{RT} \quad (21)$$

From the second of Equations (4) on page 6,

$$\rho = \rho_w - s(\rho_w - \rho_a)$$

Using Equation (7) gives

$$\rho_w - \rho = \frac{Q_a}{Q}(\rho_w - \rho_a)$$

and noting that $Q_a = m_a/\rho_a$,

$$\rho_w - \rho = \frac{m_a}{Q} \left(\frac{\rho_w}{\rho_a} - 1 \right)$$

Substituting this into the definition of the buoyancy flux F in Equation (19) gives

$$F = m_a g \left(\frac{\rho_w}{\rho_a} - 1 \right) \quad (22)$$

Non-dimensionalization

Define scaling factors λ such that $\xi = \lambda_\xi \bar{\xi}$ where ξ is any variable and an overbar represents a non-dimensional value. Substituting into Equations (17) and (19) - (21) gives

$$\begin{aligned}
\frac{\lambda_z}{\lambda_t} &= \lambda_w & \frac{\lambda_M}{\lambda_t} &= \lambda_F \\
\lambda_M &= \lambda_\rho \lambda_Q \lambda_w & \frac{\lambda_Q}{\lambda_t} &= \lambda_w^2 \\
\lambda_P &= \lambda_\rho \lambda_z & \lambda_\rho &= \frac{\lambda_P}{\lambda_{RT}}
\end{aligned} \tag{23}$$

Note that Equations (18) result in an identity and the second of Equations (20) gives a redundant relationship. Equations (23) are 6 equations in 9 unknowns, so 6 of the unknowns can be determined in terms of the other three. Distances, densities, and buoyant forces will be $O\{1\}$ by selecting the following:

$$\boxed{
\begin{aligned}
\lambda_z &= H \\
\lambda_\rho &= \rho_w \\
\lambda_F &= F_o = (\rho_w - \rho_{ao})gQ_{ao}
\end{aligned}
} \tag{24}$$

With these definitions, the remaining scaling factors can be determined as

$$\boxed{
\begin{aligned}
\lambda_w &= \left(\frac{F_o}{\rho_w}\right)^{1/3} & \lambda_t &= H\left(\frac{\rho_w}{F_o}\right)^{1/3} & \lambda_Q &= H\left(\frac{F_o}{\rho_w}\right)^{1/3} \\
\lambda_P &= \rho_w H & \lambda_{RT} &= H
\end{aligned}
} \tag{25}$$

Substituting the scaling factors into the governing equations gives

$$\frac{d\bar{z}}{d\bar{t}} = \bar{W} \tag{26}$$

$$\begin{aligned}
\bar{Q} &= \bar{Q}_a + \bar{Q}_w \\
\bar{m} &= \bar{m}_a + \bar{Q}_w \\
\bar{m}_a &= \text{const}
\end{aligned} \tag{27}$$

$$\frac{d\bar{M}}{d\bar{t}} \equiv \frac{d}{d\bar{t}}(\bar{\rho}\bar{Q}\bar{W}) = \bar{F} \tag{28}$$

$$\frac{d\bar{Q}_w}{d\bar{z}} = \alpha \bar{W} \quad \text{or} \quad \frac{d\bar{Q}_w}{d\bar{t}} = \alpha \bar{W}^2 \tag{29}$$

$$\bar{\rho}_a = \frac{\bar{P}}{\bar{RT}} = \frac{1 - \bar{z} + \bar{P}_{amm}}{\bar{RT}} \tag{30}$$

Noting that $\frac{d}{dt} = \frac{d}{dz} \frac{dz}{dt}$, Equations (26) and (28) may be combined to give

$$\frac{d\bar{M}}{d\bar{z}} = \frac{\bar{F}}{\bar{W}} \quad (31)$$

Differentiate the second of Equations (27), remembering that m_a is a constant, to give

$$\frac{d\bar{m}}{d\bar{z}} = \frac{d\bar{Q}_w}{d\bar{z}} \quad (32)$$

Then the first of Equations (29) becomes

$$\frac{d\bar{m}}{d\bar{z}} = \alpha \bar{W} \quad (33)$$

The buoyancy flux F is determined in Equation (22). Dividing both sides by $\lambda_F = F_o$, remembering that $Q_{ao} = m_a/\rho_{ao}$, and rearranging gives

$$\bar{F} = \frac{\bar{\rho}_{ao}}{\bar{\rho}_a} \frac{1 - \bar{\rho}_a}{1 - \bar{\rho}_{ao}} \approx \frac{\bar{\rho}_{ao}}{\bar{\rho}_a} \quad (34)$$

Since the density of air is so much smaller than the density of water, the factor

$\kappa \equiv \frac{1 - \bar{\rho}_a}{1 - \bar{\rho}_{ao}} = \frac{\rho_w - \rho_a}{\rho_w - \rho_{ao}}$ is very close to 1. Substituting numerical values for the density of water and the

density of air as a function of z [as given by Equation (21)] shows that as z varies from 0 to 200 ft, κ varies from 1.0 to 1.0075. Hence the approximate equality in Equation (34).

Noting that $W = M/m$, the non-dimensional governing equations are

$$\frac{d\bar{m}}{d\bar{z}} = \alpha \bar{W} \quad (33)$$

$$\frac{d\bar{M}}{d\bar{z}} = \frac{\bar{\rho}_{ao}}{\bar{\rho}_a} \bar{W} \quad (35)$$

$$\bar{\rho}_a = \frac{\bar{P}}{\bar{R}\bar{T}} = \frac{1 - \bar{z} + \bar{P}_{am}}{\bar{R}\bar{T}} \quad (30)$$

$$\bar{W} = \frac{\bar{M}}{\bar{m}} \quad (36)$$

The first two of these equations are a system of differential equations in M and m which define an initial value problem. The second two define quantities appearing on the right hand side of the first two.

Once this system of equation has been solved numerically, the quantities of interest for this study must be determined. Substitute $Q = m/\rho$ into the first of Equations (18), and apply the scaling factors from Equations (24) and (25). The result is

$$\bar{Q} = \frac{\bar{m}_a}{\bar{\rho}_a} + \bar{m}_w \quad (37)$$

The volume fraction of air, s , is defined by Equation (7) on page 7 as

$$s = \frac{Q_a}{Q} = \frac{\bar{Q}_a}{\bar{Q}} = \bar{s} \quad (7)$$

Noting that the first term on the right-hand-side of Equation (37) is \bar{Q}_a , s can be written as

$$\bar{s} = \frac{1}{1 + \bar{\rho}_a \left(\frac{\bar{m}}{\bar{m}_a} - 1 \right)} \quad (38)$$

Note that the dimensional s in Equation (7) and the non-dimensional \bar{s} in Equation (38) will have the same numerical value. Once the value of s is determined, Equations (8) and (10) on page 7 give the plume acoustic properties of interest.

Another property which will turn out to be of interest is the time required for the Lagrangian volume element to reach the surface, t_s . This is obtained by numerical integration of Equation (26).

$$\bar{t}_s = \int_0^1 \frac{d\bar{z}}{\bar{W}} \quad (39)$$

The dimensional value is then

$$t_s = \lambda_t \bar{t}_s = H \left(\frac{\rho_w}{F_o} \right)^{1/3} \bar{t}_s \quad (40)$$

Relationship of Top Hat and Actual Velocity Profiles

Dimensional analysis and laboratory measurements of mean velocities in a turbulent buoyant plume have shown the flow to be self-similar and well represented by a Gaussian profile. That is,

$$w = w_m e^{-\frac{y^2}{b^2}} \quad (41)$$

where w_m is the maximum, or centerline, velocity and b is the width of the profile. Dimensional analysis shows b to be proportional to height above the nozzles, and experiments have shown

$$b = 0.116z \quad (42)$$

Note that when $y = b$, $w = e^{-1}w_m$.

Equating the mass and momentum flux of the Top Hat velocity profile and the actual profile gives the following relations [Lee and Chu (2003)]

$$\begin{aligned} w_m &= 2W \\ b &= \frac{B}{\sqrt{2}} \end{aligned} \quad (43)$$

The concentration, or volume fraction, of air in the rising plume has been found to follow a self-similar Gaussian distribution, similar to that for velocity

$$s = s_m e^{-\frac{y^2}{(\lambda b)^2}} \quad (44)$$

where b = width of the velocity profile, and

$$\lambda = 1.35 \quad (45)$$

The maximum value of s_m in Equation (44) is given in terms of average \bar{s} , Equation (38), by

$$s_m = 1.25\bar{s} \quad (46)$$

Specific Momentum Flux and Characteristic Length of Buoyant Jet Flow

A jet is the flow produced by a continuous source of momentum. A plume is the flow produced by a continuous source of buoyancy. In our case, as air exits from the nozzle at a relatively high velocity, it is a continuous source of both momentum and buoyancy, and so we have a buoyant jet. Lee and Chu (2003) show through dimensional analysis and experimental results that the majority of the flow produced by a buoyant jet is controlled by buoyancy.

In order to quantify exactly which part of the flow is controlled by buoyancy, it is necessary to compare the momentum flux with the buoyancy flux. The specific momentum flux (that is, momentum flux per unit mass) at the nozzle exit is given by

$$M_{so} = \frac{M_o}{\rho_{ao}} = Q_{ao} w_o \quad (47)$$

where w_o is the velocity of the air at the nozzle exit. Similarly, the specific buoyancy flux is

$$F_{so} = \frac{F_o}{\rho_{ao}} = \frac{(\rho_w - \rho_{ao})}{\rho_{ao}} g Q_{ao} \quad (48)$$

The characteristic length of a two-dimensional buoyant jet is given by

$$l_s = \frac{M_{so}}{F_{so}^{2/3}} \quad (49)$$

Experiments have shown that the flow in a two dimensional buoyant jet is plume-like for

$$\frac{z}{l_s} \geq 4 \quad (50)$$

“Plume-like” means that above 4 characteristic lengths, the initial momentum of the jet exiting the nozzles is completely dissipated, and only buoyancy controls the flow.

Compressible Fluid Flow Through the Nozzles

The manifold and nozzles essentially are in an infinite heat sink – the ocean. Assume the air in the manifold has been in transit long enough to reach the ocean temperature. The nozzles are short, so take the flow through the nozzles to be an isentropic flow of a perfect gas [Obert (1948), Binder (1951), Beychok (2008)].

Let k = the ratio of specific heats, equal to 1.4 for air.

P_M = Pressure in the manifold

P_o = External pressure at the nozzle exit

T_{sw} = Temperature of the air in the manifold = temperature of the seawater in °R

R = the gas constant = 53.36 ft-lb_f/lb_m-°R for air.

Then, for subsonic velocities, the mass flow rate through a single nozzle, m_o , is

$$m_o = C_{dss} a P_M \sqrt{\frac{2g}{RT_{sw}} \left(\frac{k}{k-1} \right) \left[r_p^{2/k} - r_p^{(k+1)/k} \right]} \quad \text{Subsonic} \quad (51)$$

where a is the exit area of the nozzle, C_{dss} is the subsonic discharge coefficient, and the pressure ratio, r_p , is defined as

$$r_p \equiv \frac{P_o}{P_M} \quad (52)$$

Using the isentropic pressure-density relationship

$$\frac{P}{\rho^k} = \text{Const} \quad (53)$$

it may be shown that there exists a critical pressure ratio, r_{pc} , for which the mass flow rate based on the velocity given by Equation (51) reaches a maximum.

$$r_{pc} = \left(\frac{2}{k+1} \right)^{\frac{k}{k-1}} \quad (54)$$

This velocity at the critical pressure ratio, r_{pc} , is the sonic velocity, and no matter how far r_p is decreased below r_{pc} , the velocity does not increase. In our case, no matter how much P_m is increased, the exit velocity will not increase. However, as P_m is increased, the mass flow rate, m_o , continues to increase, and is given by

$$m_o = \frac{C_{ds} a P_m}{\sqrt{T_{sw}}} \sqrt{\frac{gk}{R} \left(\frac{2}{k+1} \right)^{\frac{k+1}{k-1}}} \quad \text{Sonic Flow} \quad (55)$$

where C_{ds} is a sonic discharge coefficient, which is highly dependent on the exact shape of the nozzle or orifice through which a gas is flowing.

Volume flow rate through the nozzle is then given by

$$q_o = \frac{m_o}{\rho_{ao}} \quad (56)$$

where ρ_{ao} is the density of the air at the nozzle exit. Exit velocity is

$$w_o = \frac{q_o}{a} \quad (57)$$

Air density in the manifold is determined from the perfect gas law. If the air is at the seawater temperature, T_{sw} , then

$$\rho_{aM} = \frac{P_M}{RT_{sw}} \quad (58)$$

Manifold Design

Kreinin and Kafyrin (1979) give equations for the design of isothermal distributing manifolds. These equations will be used to determine the minimum manifold diameter necessary to limit the pressure drop between the first nozzle and the last nozzle.

The manifold inlet Reynolds number is given by

$$\text{Re}_{in} = \frac{V_{in} D}{\nu} \quad (59)$$

where V_{in} is the air velocity at the beginning of the manifold

D is the manifold diameter

ν is the kinematic viscosity of the air at the manifold inlet.

As stated by Edwards (2003), the viscosity of air, μ , is a function primarily of temperature. It varies very little with pressure. The Sutherland formula for viscosity is

$$\mu = \mu_o \left(\frac{a}{b} \right) \left(\frac{T}{T_o} \right)^{3/2} \quad (60)$$

where $a = 0.555T_o + C$

$$b = 0.555T + C$$

μ_o = reference μ at reference temperature T_o

C = Sutherland's constant.

For standard air, $C = 120$

$$T_o = 524.07^\circ R$$

$$\mu_o = 0.01827 \text{ cp}$$

Kinematic viscosity, ν , is given by

$$\nu = \frac{\mu}{\rho} \quad (61)$$

V_{in} is given by the total volume rate of air flow divided by the manifold area. Using Equation (13) and the usual formula for the area of a circle, Re_{in} can be written as

$$Re_{in} = \frac{4nq_o L_M}{\pi\nu D} \quad (62)$$

Define a quantity η as

$$\eta = \frac{Re_{in} D}{16 L_M} = \frac{nq_o}{4\pi\nu} \quad (63)$$

Then a friction factor F can be defined as

$$F^2 = \left| \frac{2}{\eta} (1 + \eta) - \frac{\alpha_M}{2} \right| \quad (64)$$

where $\alpha_M = 2$ for $Re \leq 2300$ and $\alpha_M = 1.05 - 1.1$ for $Re > 2300$.

The total exit area of all the nozzles is given by

$$a_\Sigma = nL_M \frac{\pi d^2}{4} \quad (65)$$

where d is the nozzle diameter. The ratio of the nozzle area to the manifold area is

$$\hat{a}_\Sigma = \frac{a_\Sigma}{\pi D^2 / 4} \quad (66)$$

If $F\hat{a}_\Sigma$ is small, then the ratio of the pressure at the end of the manifold to the pressure at the beginning of the manifold is given by

$$\frac{P_{end}}{P_{in}} = 1 - (F\hat{a}_\Sigma)^2 \quad (67)$$

From Equation (66), it is obvious that P_{end}/P_{in} depends on the ratio of total nozzle exit area to manifold cross section area.

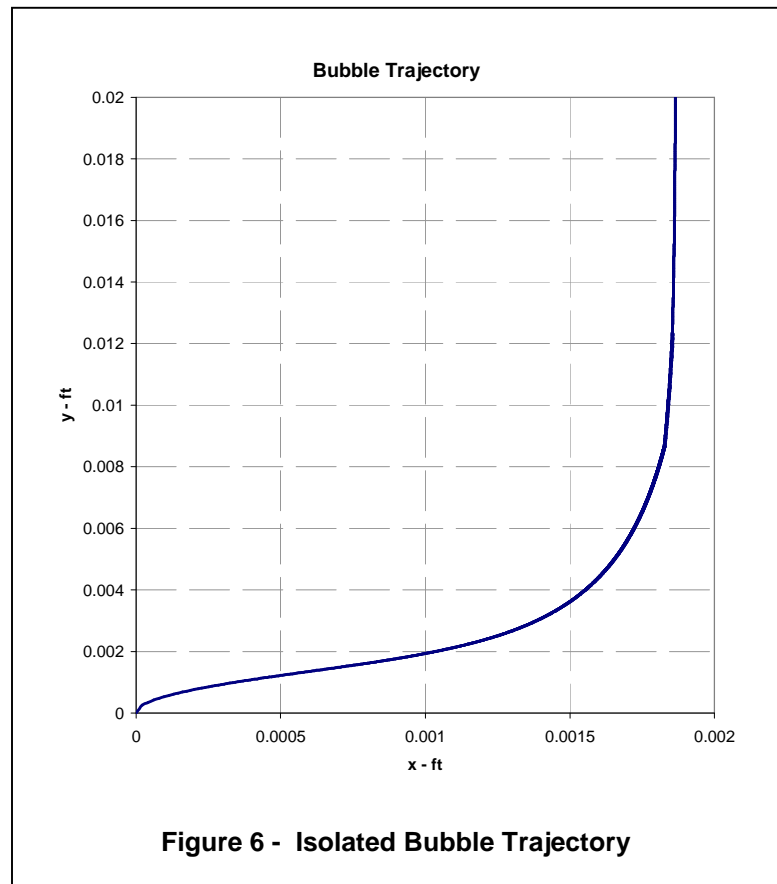
Calculation of Manifold Length

All formulations to this point have been for a stationary manifold discharging air into still water. The assumption of still water may be accurate enough, but towing a manifold behind a seismic survey vessel traveling at 5 kts is far from stationary. So the question is, just what effect will the manifold traveling at 5 kts have on the formulation to this point.

The answer is ultimately found in the Lagrangian formulation described in "Lagrangian Analysis" on page 9. However, the analysis described in Appendix B provides some guidance. Appendix B analyzes a single, isolated bubble of air, 1/4-inch in diameter, ejected at high velocity (100 fps) from a manifold traveling at 5 kts. This analysis has no direct application to the design of a towed manifold for the production of an air curtain. But it does illustrate how rapidly the horizontal and vertical velocity of this isolated bubble is reduced.

The trajectory of the bubble is shown in Figure 6. This plot shows that the bubble moves less than 0.002 ft in the direction of manifold travel. At the same time, the bubble has risen about 0.02 feet above the manifold nozzle exit. The results shown in this bubble trajectory confirm that the motion of a manifold moving at a velocity of 5 kts may be neglected.

Now consider the volume element in Figure 5. Just as for the single isolated bubble, as soon as the element moves up away from the nozzle, it is completely disengaged from the traveling manifold. The only forces then acting on it are caused by its momentum traveling through the still water and its buoyancy. Equation (50) on page 15 shows the vertical momentum is dissipated in a relatively short distance. And since the volume element of the jet is much larger than the 1/4-inch bubble in Appendix B, the horizontal momentum should also dissipate rapidly.



OPTIMAL DESIGN

All the equations necessary for the design of an air curtain have been stated in the previous sections. But the sheer number of equations and the interdependencies involved make any effort to arrive at a reasonable design very difficult. Fortunately, optimization methods exist for attacking just this sort of problem.

Principles

A brief summary of optimal design, adapted from Papalambros and Wilde (1988), follows.

The goal of design optimization is to improve a design so as to achieve the best way of satisfying the original need, within the available means.

A more rigorous statement is that design optimization involves:

- The selection of a set of variables to describe the design alternatives
- The selection of an objective, or criterion, expressed in terms of the design variables, which we seek to minimize or maximize
- The determination of a set of constraints, expressed in terms of the design variables, which must be satisfied by any acceptable design
- The determination of a set of values for the design variables, which minimize (or maximize) the objective, while satisfying all the constraints

The set of design variables is collectively known as the "*State Variable*"; it is an array of the independent variables chosen to describe the design alternatives. When the values of these variables are known (or assumed), everything else about the system can be calculated.

The objective of the design is known as the "objective function", and it is a function of the State Variable.

The constraints are represented by functional relations among the design variables (the State Variable) such as

$$h(\mathbf{x}) = 0$$

$$g(\mathbf{x}) \geq 0$$

where \mathbf{x} is the State Variable and $h()$ and $g()$ represent functions. As indicated by the equations, there are *equality constraints* and *inequality constraints*.

Application to Air Curtain Design

The principles stated above can be easily implemented in an Excel workbook using the Excel Solver add-in. Certain input quantities are required, such as water properties, air properties, depth of manifold below surface, number and diameter of nozzles, etc. With these values known, the state vector is taken to be composed of manifold pressure and manifold diameter.

$$\text{State Vector} = \begin{bmatrix} P_M \\ D \end{bmatrix} \quad (72)$$

Using the input values and P_M , the air flow through a nozzle can be calculated; the plume equations then determine the value of the air volume fraction in the plume; and the speed of sound ratio and specific impulse ratios can be calculated. Using D and the quantities already calculated, the pressure drop in the manifold can be calculated.

The objective function to be minimized is taken to be the pneumatic power of the flow in the manifold, that is, pressure times flow rate:

$$Power = P_M Q_{\sigma T} \quad (73)$$

An equality constraint is used to determine the manifold diameter, D . The calculated ratio of the pressure at the end of the manifold, P_{end} , to the pressure at the beginning of the manifold, P_{in} , is set equal to some allowable value, chosen by the user. In this case the allowable value was chosen to be 0.98.

$$\frac{P_{end}}{P_{in}} - \left(\frac{P_{end}}{P_{in}} \right)_{Allowable} = 0 \quad (74)$$

Obviously, the manifold pressure must be greater than or equal to the external pressure or there will be no flow. At the same time, the pressure at the end of the manifold must also be greater than the external pressure. In fact, it should be some specified value greater than the external pressure. This minimum allowable pressure differential is chosen to be 2 psi.

In order to attenuate the air gun noise, the velocity of sound in the bubble plume, c , must be less than the velocity of sound in water, c_w . So the ratio c/c_w is constrained to be less than some selected value of $(c/c_w)_{max}$.

Thus the set of inequality constraints is

$$\begin{aligned} \text{Manifold Pressure} - \text{External Pressure} &\geq 0 \\ (\text{Manifold End Pressure} - \text{External Pressure}) - \text{Allowable Differential} &\geq 0 \\ \left(\frac{c}{c_w} \right)_{max} - \frac{c}{c_w} &\geq 0 \end{aligned} \quad (75)$$

Equations (72) through (74) present a well-defined optimization problem. However, the calculations for the plume involve numerical solution of the Equations (30), (33), (35), and (36) on page 12.

The numerical solution was achieved by using a fourth-order Runge-Kuta routine for systems of initial value differential equations [Faires and Burden (1993)]. This routine was programmed as a user function in VBA. Integration is performed from the manifold to the surface ($\bar{z} = 0$ to 1). At each step, the c/c_w ratio is calculated, and compared with the maximum c/c_w ratio already obtained. At conclusion of the integration, the function returns the maximum c/c_w ratio for use in the last constraint of Equation (75).

This completes the definition of the optimization problem. These equation have been programmed into the Excel workbook, Air Curtain Design.xls. This workbook is described in more detail in Appendix C, and comparisons of the workbook formulas for calculation of air flow rates with experimental results is described in Appendix D.

RESULTS

Naturally, results depend on values of the input quantities. Sheet "Input" of the Air Curtain Design.xls workbook, containing all input values, is shown in Appendix C. Before presenting results, it is worthwhile to call attention to some of these input values.

Values for all the properties of air are standard values. The density of the sea water is taken to be constant at $64 \text{ lb}_m/\text{ft}^3$ and its temperature is taken to be 40°F .

The manifold is envisioned to be similar to a "fire hose", so that it can be rolled up in its flattened configuration. When deployed, air pressure expands it to a circular shape. This concept does not allow for nozzles of any length, so the "nozzles" are treated as orifices. Accordingly, the nozzles discharge coefficients are taken to be 0.65.[J. E. Gasho & Associates (unknown)]

The vessel speed is taken to be 5 kts, or 8.4 fps, and the array length is taken to be 50 ft. The extra length Δ [see Figure 7] is taken to be 10 ft.

The minimum pressure drop ratio in the manifold is taken to be 0.98; that is, the pressure at the end of the manifold has dropped only 2% below the pressure at the beginning of the manifold. Also the minimum pressure differential at the end of the manifold is taken to be 2 psi. That is, the pressure at the end of the manifold is at least 2 psi greater than the external pressure. Later detailed design will have to seriously evaluate these input values, because the manifold diameter and length depend heavily on both.

With all other input values established, it is necessary to choose the depth of the manifold, H ; the diameter, d ; and number per foot, n , of the nozzles (orifices); and a desired maximum value of the c/c_w ratio. Using the Solver add-in of Excel, a manifold pressure and diameter are determined which meet all constraints and minimize the pneumatic horsepower. Thus there is a solution for each combination of these variables.

So a matrix of solutions has been generated. At the end of each Solver minimization process, significant results were copied onto a row in the matrix. The complete matrix is contained in Sheet "SolutionSummary" of the workbook and presented in its entirety in Appendix E.

Selection of a "Best" Design

This investigation is based achieving a c/c_w ratio as small as possible, without actual calculation of the resulting attenuation of the air gun pressure signal. No details of the manifold deployment system were investigated, so no calculations of pressure loss from the air compressor to the beginning of the manifold and the first nozzle were made. No heat transfer calculations were made, so the actual air temperature in the manifold was assumed. In addition, no investigation into air compressor specifications was conducted.

Within these limitations, "the best" design can be defined as that which produces the largest volume of air, using the least horsepower, and with the smallest manifold diameter, all of which are mutually exclusive. As in any design problem, the design designated as "the best" in this investigation is a result of compromise among conflicting requirements. Without the further detailed specification of various parts of the system to produce the air curtain, picking the "best" design is a matter of engineering judgment.

Pneumatic horsepower and manifold diameter were chosen as the primary variables of interest. Secondary variables included volume flow rate, manifold length, and towing position with respect to the air gun array. To illustrate the application of engineering judgment to the matrix of solutions, consider Figure E - 1 from Appendix E, reproduced below as Figure 9.

This figure shows pneumatic hp and manifold diameter plotted against the maximum c/c_w ratio for a manifold depth of 200 ft, the maximum depths of the Beaufort and Chukchi Seas. Solutions are plotted for various number and diameter of nozzles.

Immediately obvious is the fact that all the solid hp curves have values greater than about 1000 hp. It is not possible to accept a higher maximum value of c/c_w in order to require less hp because the lowest point on each hp curve has reached the minimum pressure differential constraint at the end of the manifold. Lower hp can only be achieved by allowing pressure in the manifold at its end to be less than 2 psi greater than the external pressure!

Ideally, the maximum c/c_w ratio would be less than 0.1; that is, the speed of sound in water would be at least 10 times the speed of sound in the plume. None of the values in this figure approach this value.

The manifold diameter curves (dotted) in this figure range from 13 to over 24 inches.

Note that as the require hp decreases, the required manifold diameter increases. Also, as the total area of the nozzles per ft increases, the manifold diameter increases. Thus requirements for small hp and small diameter are mutually exclusive.

As can be seen in Table E - 5 and Table E - 6 of Appendix E, flow rates range from 13,200 to 56,100 scfm and manifold lengths range from 380 to 680 ft.

Figure 9 has illustrated trends in the solutions. However, it is also obvious that the requirements for the primary variables, hp and diameter, are too large for such an air curtain system to be practical. In addition, the secondary variables are too large to be practical. So shallower depths were investigated. Figures similar to Figure 9 for other depths are included in Appendix E.

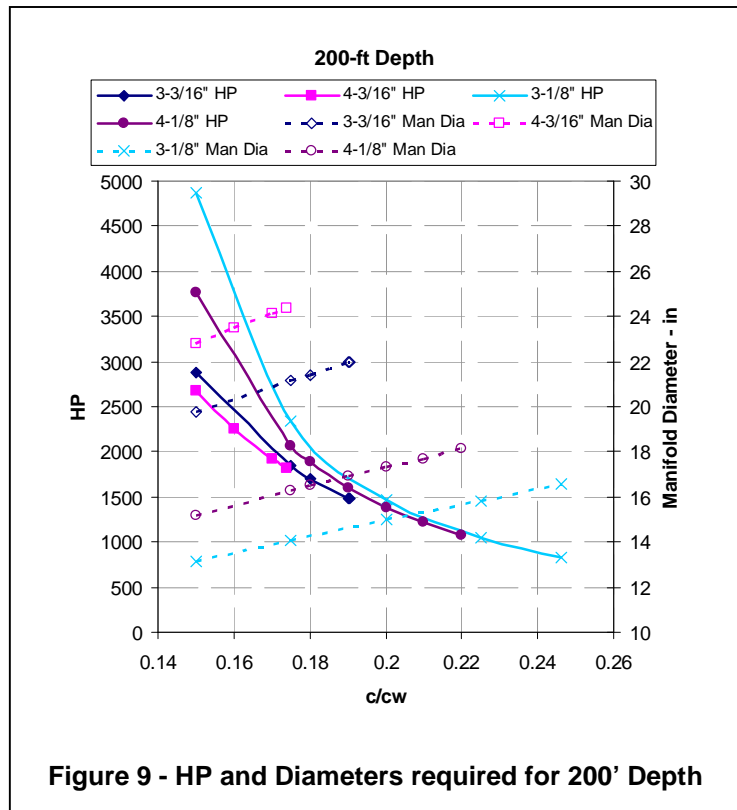
Table 1 shows the range of manifold diameters in the solution matrix for each nozzle size. Obviously the larger nozzle size requires a larger manifold diameter. The same effect is obtained when the number of nozzles per foot is increased.

MANIFOLD DIA RANGE		
Nozzle Dia (in)	Manifold Dia	
	Min (in)	Max (in)
0.125	7.108	18.289
0.1875	10.493	24.365

So required horsepower can be reduced by increasing either the nozzle size or the number of nozzles per foot. But reduced horsepower comes at the cost of increased manifold diameter and all the associated practical handling problems.

The recommended system is shown as Solution #58, highlighted in orange, in Table E - 2 of Appendix E. This design is for a manifold having 3 – 1/8” nozzles per ft at a depth of 60 ft producing a maximum c/c_w ratio of 0.07.

Such a system requires 423 hp, a flow rate of 4933 scfm, and a manifold diameter of 9”. Manifold length is 201 ft, and it should be towed 141 ft in front of the air gun array.

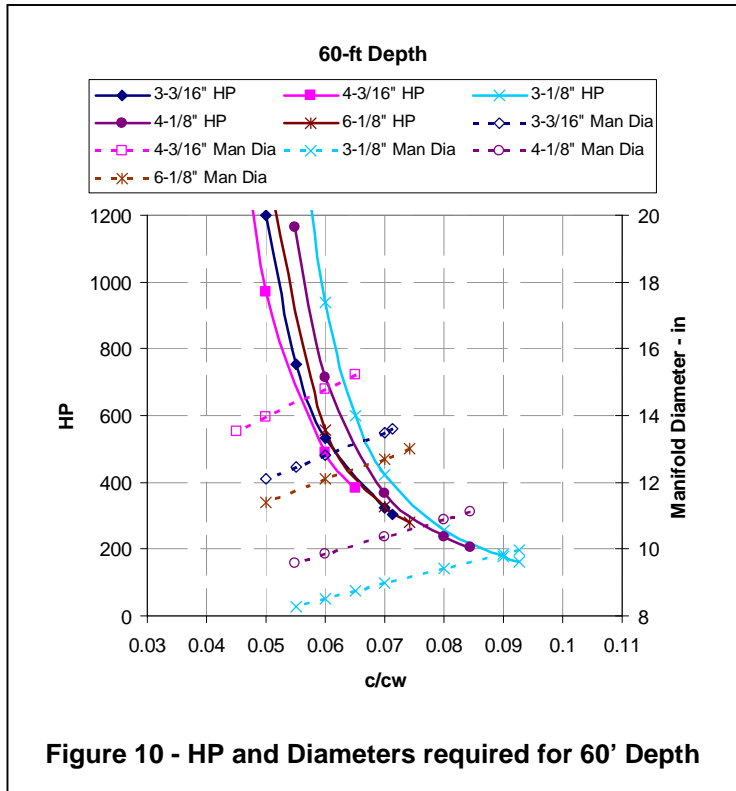


The hp and manifold diameter plot from Figure E - 5 is reproduced here as Figure 10. The recommended system is represented by a point at $c/c_w = 0.7$ on the light blue curves which have an "x" for each data point.

A similar system is that of Solution #64 in Table E - 2 of Appendix E, also shown in Figure 10. This manifold has 4 -1/8" nozzles per ft, requires 367 hp, 4924 scfm, a manifold diameter of 10.4", and produces a maximum c/c_w ratio of 0.07. Solution #58 is recommended over this system because the manifold diameter is about an inch and a half smaller. The power required for Solution #58 is about 50 hp more, but 50 hp may be "cheaper" than handling and deploying a larger manifold. Manifold length is the same for both cases.

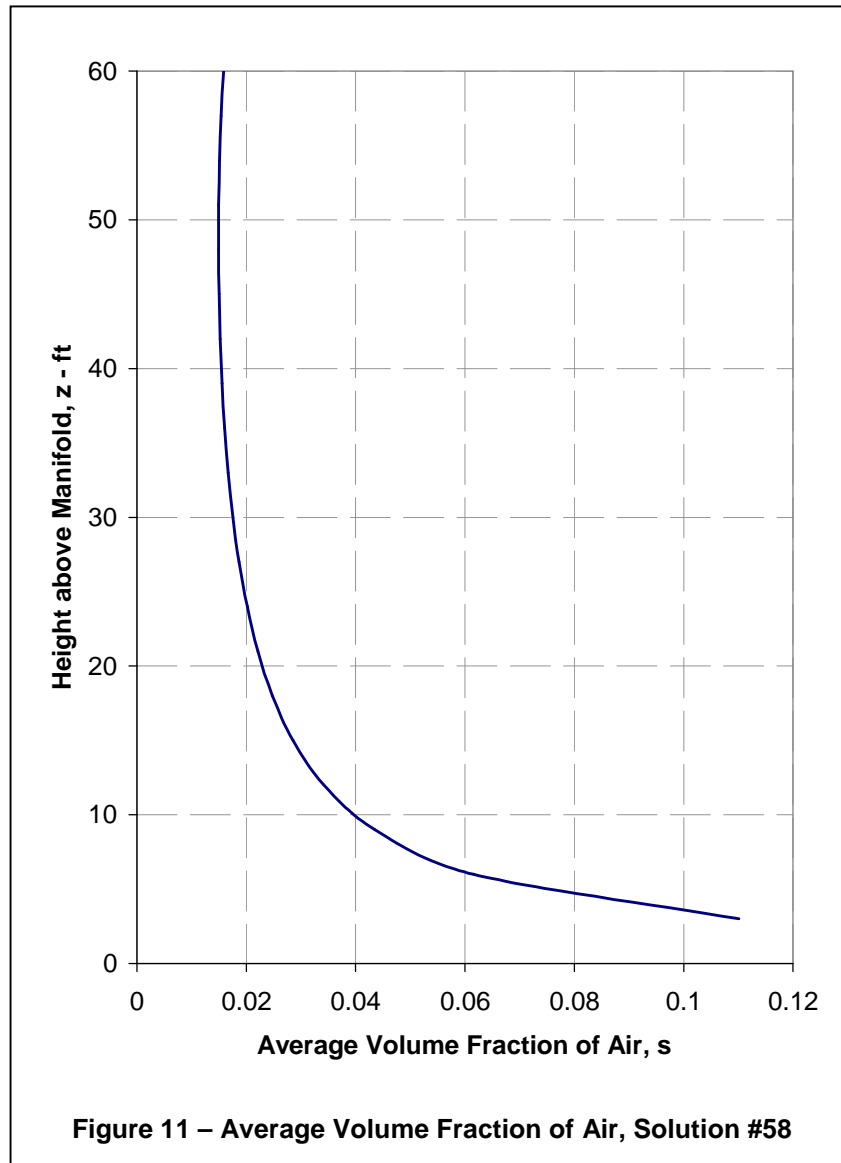
Detail investigation of the pressure signal attenuation properties of the air curtain produced by the selected manifold may call for different compromises among the conflicting requirements for the design.

For example, it may be worth using a compressor with more horsepower in order to get better signal attenuation. For the present, the selected "best" design represents a realistic starting point for more detailed investigation.



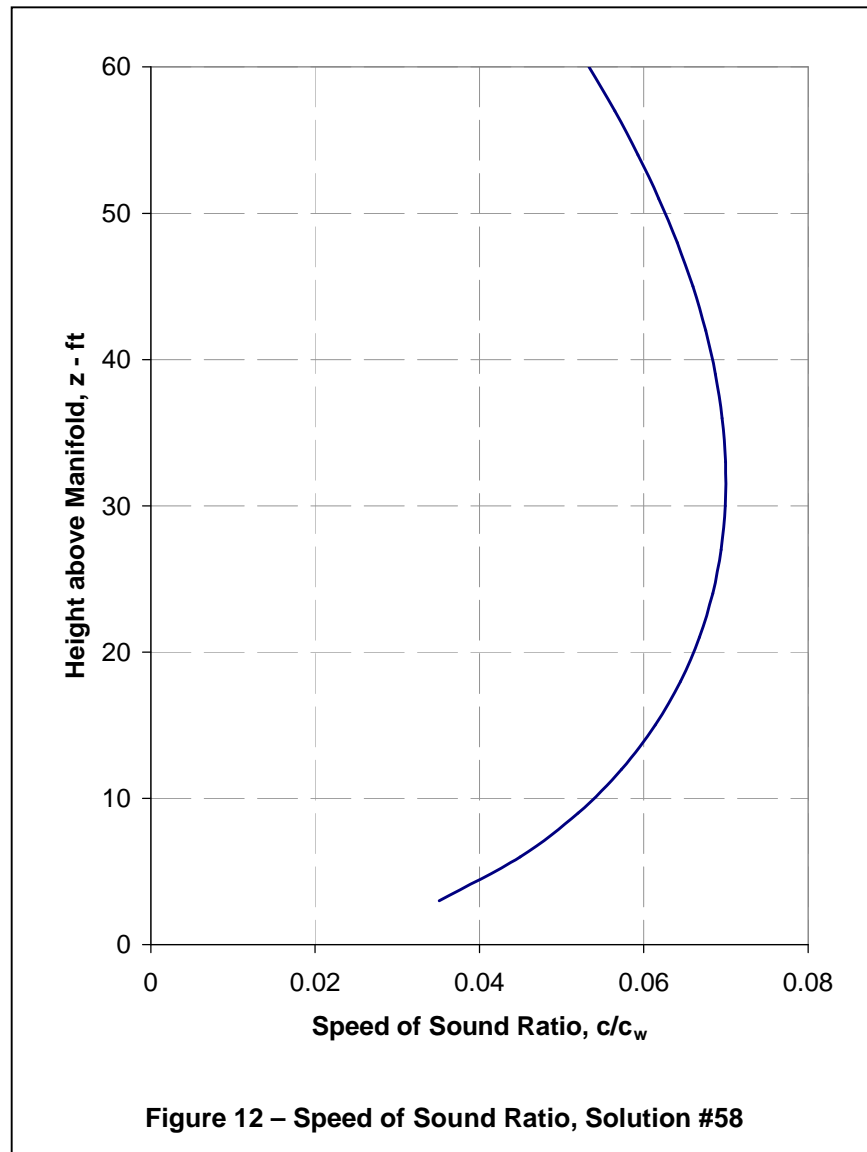
Discussion of Selected System

The variation in volume fraction of air as a function of height above the manifold for Solution #58 is shown in Figure 11. At the nozzle exit, the volume fraction of air is 1.0. As this figure shows, at a height, z , of 3 ft above the nozzle exit, the average volume fraction has already been reduced to 11%. This reduction is due to the water entrained in the upward flow. The fraction continues to decrease to a minimum of about 1.5% at $z = 48$ ft, and then slightly increases from there to the surface. This increase is due to the



expansion of the air having a greater effect than the entrainment of water into the flow.

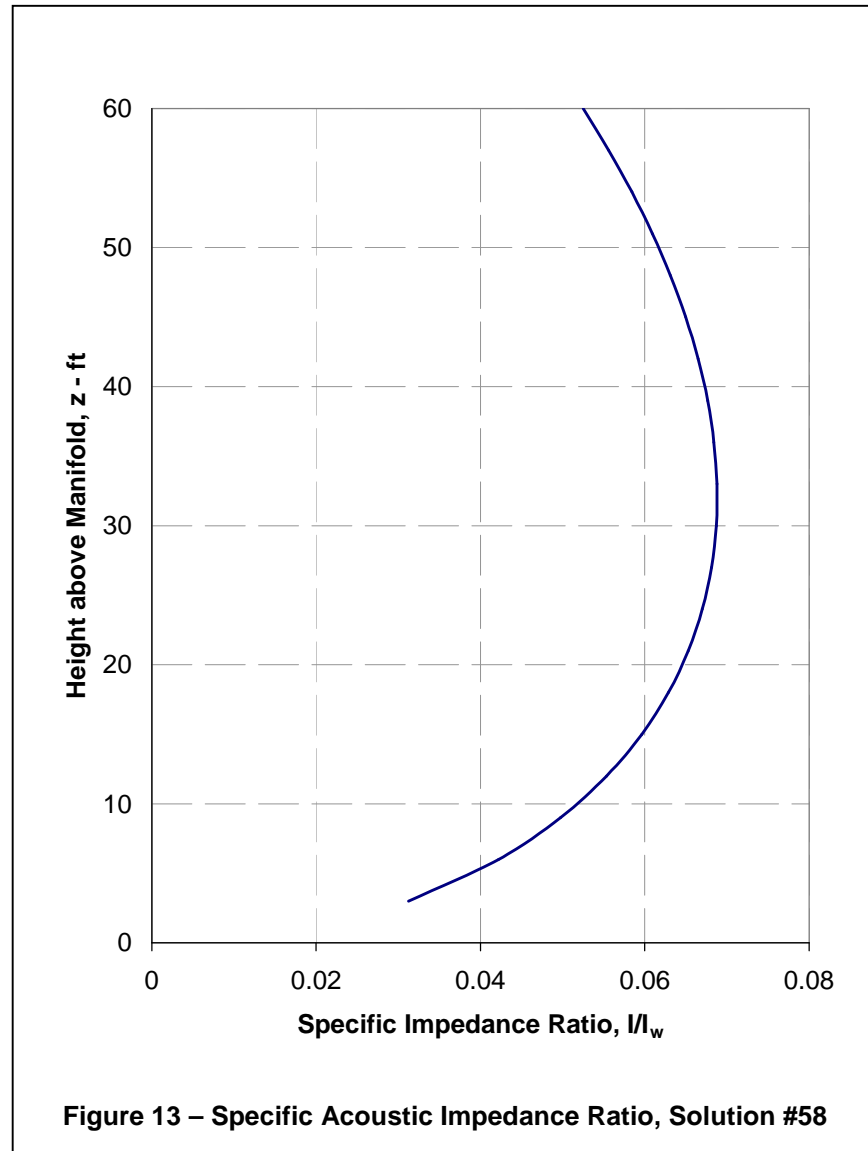
The variation in the speed of sound ratio, c/c_w , as a function of height above the manifold for Solution #58 is shown in Figure 12. At 3 ft above the manifold, it is 0.035; it reaches a maximum value of 0.07 at a



height of 31.7 ft above the manifold; and decreases to 0.053 at the surface.

This relatively wide variation occurs even though the average volume fraction of air, s , is almost constant from mid-depth to the surface. However, when the formula for calculating c/c_w , shown in Equation (8) on page 7 is considered, it is obvious that the dependence on z is a complex one. The variation in s is shown in Figure 11. At the same time both compressibility, β_a , [Equation (6) and the second equality in Equation (21)] and density, ρ_a , [Equation (21)] of the air vary with z . The result is shown in the figure.

The variation in the specific acoustic impedance, I/I_w , as a function of height above the manifold for Solution #58 is shown in Figure 13. As shown at the end of Appendix C, this curve is simply ρ/ρ_w times the c/c_w curve, So the shape of the curves in Figure 13 and Figure 12 is very similar, and the values are close.



REFERENCES

- Anonymous (1996), "Bubble Screen Acoustic Attenuation Test #1 Conducted for Shell Venezuela", Western Geophysical, Western Atlas International, Inc, Houston, TX.
- Ayers, Ray R. (2007), "Methods to Reduce Lateral Noise Propagation from Seismic Exploration Vessels", PN 117168, Stress Engineering Services, Inc. proposal to the Minerals Management Service, Houston, Texas.
- Beychok, Milton R. (2008), Gas Discharge to the Atmosphere from a Pressure Source, <http://www.air-dispersion.com/usource.html>, (accessed October 20, 2008).
- Binder, R. C. (1951), Advanced Fluid Dynamics and Fluid Machinery, Prentice-Hall, Inc., New York.
- Costigan, G. and Whalley, P. B. (1997), "Measurements of the Speed of Sound in Air-Water Flows," Chemical Engineering Journal, Vol. 66, pp. 131-135.
- Domenico, S. N. (1982), "Acoustic Wave Propagation in Air-Bubble Curtains in Water - Part I: History and Theory," Geophysics, Vol. 47 (3), pp. 345-353.
- Edwards, Ken (2003), Gas Viscosity, <http://www.lmnoeng.com/Flow/GasViscosity.htm>, (accessed October 10, 2008).
- Faires, J. Douglas and Burden, Richard L (1993), Numerical Methods, PWS Publishing Company, Boston.
- J. E. Gasho & Associates, Inc. (unknown), Application Engineering Basics, <http://www.jegasho.net/rotron%20pages/orifice%20flow%20calculation.htm>, (accessed October 30, 2008).
- Jones, Warren T. (1972), "Air Barriers as Oil-Spill Containment Devices," Society of Petroleum Engineers Journal, Vol. 12 (2), pp. 126-142.
- Jones, Warren T. (2008), Email to R. R. Ayers, "Bubble Curtain Mitigation of Lateral Noise Propagation from Seismic Exploration Vessels", September 22.
- Kreinin, E. V. and Kafyrin, Yu. P. (1979), "Design of Isothermal Distributing Manifolds," Khimicheskoe i Neftyanoe Mashinostroenie, Vol. 5, pp. 16-18.
- Lee, Joseph H. W. and Chu, Vincent H. (2003), Turbulent Jets and Plumes, A Lagrangian Approach, Kluwer Academic Publishers, Boston/Dordrecht/London.
- Obert, Edward F. (1948), Thermodynamics, McGraw-Hill Book Company, Inc., New York.
- Papalambros, Panos Y. and Wilde, Douglass J. (1988), Principles of Optimal Design, Modeling and Computation, Cambridge University Press, New York.
- Sixma, E. and Stubbs, Scott (1996), "Air Bubble Screen Noise Suppression Tests in Lake Maracaibo", Congreso Venezolano de Geofisica, Sociedad Venezolana de Ingenieros Geofisicos.
- Spence, Jesse (2008), "Seismic Array Directionality Study", Technical Memo 08-035, Noise Control Engineering, Inc.
- Sutherland, John W. (2002), Forces Acting on Airborne Particles, <http://www.mfg.mtu.edu/cyberman/environment/air/forces/forces.html>, (accessed September 20, 2008).
- Towell, G. D., Strand, C. AP., et al. (1965), "Mixing and Mass Transfer in Large Diameter Bubble Columns", A.I.Ch.E.-A.Chem.E. Symposium Series No. 10, pp. 10:97-10:105.

Appendix A

Compressibility of Air

Appendix A

Compressibility of Air

Compressibility, β , is given by

$$\beta = -\frac{dv/v}{dP} \quad (\text{A-1})$$

where v is specific volume and $v = 1/\rho$.

As the air rises toward the surface after leaving the nozzle, it is in essentially an infinite heat sink, the ocean, and turbulence ensures that the air is well mixed with the sea water. So temperature of the air should remain constant at the sea water temperature. To calculate its compressibility, write the perfect gas equation as

$$Pv = RT \quad (\text{A-2})$$

Take the differential of both sides and set $dT = 0$ since the process is isothermal.

$$Pdv + vdP = 0 \quad (\text{A-3})$$

Solving for dv/v and substituting into Equation (A-1) gives

$$\beta_a = \frac{1}{P} = \frac{1}{P(z)} \quad (\text{A-4})$$

The second equality is included to indicate that the pressure of the air rising toward the surface is a function of height above the nozzle, z .

Domenico (1982) quotes the relationship $\beta_a = 1.0086/P$ obtained from the American Institute of Physics Handbook as the actual relationship for air. Since this is a feasibility study, the perfect gas relationship of Equation (A-4) is accurate enough.

Appendix B

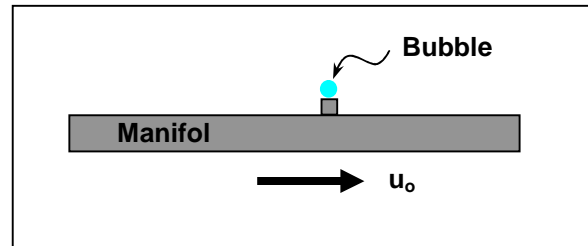
Isolated Bubble Trajectory

Appendix B

Isolated Bubble Trajectory

Consider an isolated, single bubble ejected from a manifold being towed at a speed of u_o , as shown in the adjacent sketch. At the instant the bubble exits from the nozzle, it is traveling in the x -direction at a speed of u_o and in the z direction at a velocity of w_o .

The bubble is a sphere with a $\frac{1}{4}$ -inch diameter, in accordance with the predominant bubble size in a buoyant plume of air exiting into water. For simplicity, assume the bubble does not change shape or expand with lessening pressure. With these assumptions, the bubble is essentially a solid body.



Equations of Motion

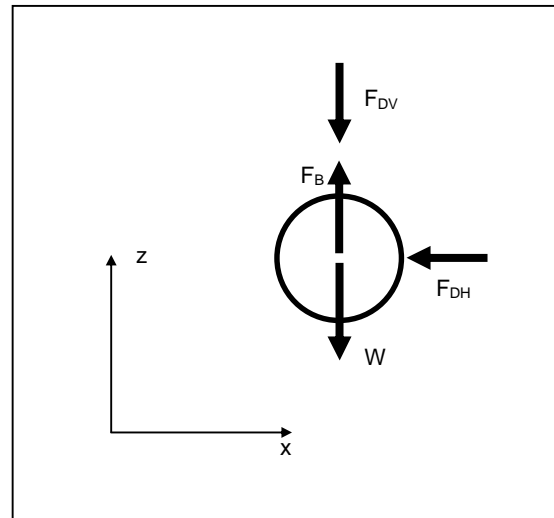
A free body of the bubble is shown in the adjacent sketch. The bubble has a weight W and is acted upon by a buoyant force F_B . Because of its velocity in the x direction, there is a horizontal drag force, F_{DH} , exerted on the bubble. Because of its velocity in the z direction, there is a vertical drag force, F_{DV} , exerted on the bubble.

The equations of motion are given by

$$\begin{aligned} m\ddot{x} &= -F_{DH} \\ m\ddot{z} &= F_B - W - F_{DV} \end{aligned} \quad (\text{B-1})$$

and initial conditions for $x(t)$ and $z(t)$ are

$$\begin{aligned} x(0) &= 0 \\ \dot{x}(0) &= u_o \\ z(0) &= 0 \\ \dot{z}(0) &= w_o \end{aligned} \quad (\text{B-2})$$



Various quantities involved in these equations are

$$\begin{aligned} m &= \frac{w_a}{g} \frac{\pi D^3}{8} & A &= \frac{\pi D^2}{4} & W &= w_a \frac{\pi D^3}{8} \\ F_B &= w_{sw} \frac{\pi D^3}{8} & \rho_{sw} &= \frac{w_{sw}}{g} \\ F_{DH} &= \frac{1}{2} \rho_{sw} C_{DH} A \dot{x}^2 \\ F_{DV} &= \frac{1}{2} \rho_{sw} C_{DV} A \dot{z}^2 \end{aligned} \quad (\text{B-3})$$

where w_a and w_{sw} are the specific weight of air and seawater, respectively

D is the bubble diameter

C_{DH} and C_{DV} are the drag coefficients in the horizontal and vertical directions. Substituting into Equations (B-1) gives

$$\begin{aligned}\ddot{x} &= -\frac{w_{sw}}{w_a} \frac{C_{DH}}{D} \dot{x}^2 \\ \ddot{z} &= \frac{w_{sw} - w_a}{w_a} g - \frac{w_{sw}}{w_a} \frac{C_{DV}}{D} \dot{z}^2\end{aligned}\tag{B-4}$$

These two second order differential equations may each be written as two first order differential equations with their associated initial conditions

$$\begin{aligned}\dot{x} &= u & , & \quad x(0) = 0 \\ \dot{u} &= -\frac{w_{sw}}{w_a} \frac{C_{DH}}{D} u^2 & , & \quad u(0) = u_o \\ \dot{z} &= w & , & \quad z(0) = 0 \\ \dot{w} &= \frac{w_{sw} - w_a}{w_a} g - \frac{w_{sw}}{w_a} \frac{C_{DV}}{D} w^2 & , & \quad w(0) = w_o\end{aligned}\tag{B-5}$$

Non-dimensional Equations of Motion

Because of the velocity squared terms, a numerical solution is appropriate. In order to carry out a numerical solution, these equations need to be non-dimensionalized. So let

$$\begin{aligned}x &= \lambda_x \hat{x} \\ z &= \lambda_z \hat{z} \\ t &= \lambda_t \hat{t}\end{aligned}\tag{B-6}$$

where the λ s are scaling factors and hats represent the non-dimensional quantity. Substituting Equations (B-6) into Equations (B-5) and setting $\lambda_x/D = \lambda_z/D = g\lambda_t^2/\lambda_z = 1$ leads to the following definition of the scaling factors

$$\begin{aligned}\lambda_x &= \lambda_z = D \\ \lambda_t &= \sqrt{\frac{D}{g}} \\ \lambda_v &= \sqrt{Dg}\end{aligned}\tag{B-7}$$

where λ_v is the scaling factor for velocity. The non-dimensional system of equations becomes

$$\begin{aligned}
\frac{d\hat{x}}{d\hat{t}} &= \hat{u} & , \quad \hat{x}(0) &= 0 \\
\frac{d\hat{u}}{d\hat{t}} &= -\frac{w_{sw}}{w_a} C_{DH} \hat{u}^2 & , \quad \hat{u}(0) &= \hat{u}_o \\
\frac{d\hat{z}}{d\hat{t}} &= \hat{w} & , \quad \hat{z}(0) &= 0 \\
\frac{d\hat{w}}{d\hat{t}} &= \frac{w_{sw} - w_a}{w_a} - \frac{w_{sw}}{w_a} C_{DV} \hat{w}^2 & , \quad \hat{w}(0) &= \hat{w}_o
\end{aligned}
\tag{B-8}$$

Numerical Integration

The simplest numerical integration scheme was chosen for implementation in an Excel workbook – Euler Numerical Integration. The second of Equations (B-8) can be written as

$$\begin{aligned}
\frac{\hat{u}_{i+1} - \hat{u}_i}{\hat{t}_{i+1} - \hat{t}_i} &= -C_1 C_{DHi} \hat{u}_i^2 \\
\text{where} & \\
C_1 &= \frac{w_{sw}}{w_a}
\end{aligned}
\tag{B-9}$$

This equation may be rearranged to solve for \hat{u}_{i+1} in terms of \hat{u}_i . Similar operations on the other Equations (B-8) give

$$\begin{aligned}
\hat{u}_{i+1} &= \hat{u}_i - C_1 C_{DHi} \hat{u}_i^2 \Delta\hat{t} \\
\hat{x}_{i+1} &= \hat{x}_i + \hat{u}_i \Delta\hat{t} \\
\hat{w}_{i+1} &= \hat{w}_i + (C_2 - C_1 C_{DVi} \hat{w}_i^2) \Delta\hat{t} \\
\hat{z}_{i+1} &= \hat{z}_i + \hat{w}_i \Delta\hat{t} \\
\text{where} & \\
C_2 &= \frac{w_{sw} - w_a}{w_a} \\
\Delta\hat{t} &= \hat{t}_{i+1} - \hat{t}_i
\end{aligned}
\tag{B-10}$$

Initial conditions provide values for time step zero ($i = 0$). Then calculation of values at successive time steps from these equations is straightforward.

The drag coefficient, C_D , for a spherical particle is defined in terms of the Reynolds number, Re , as shown in Sutherland (2002).

$$C_D = \frac{24}{Re} \quad , \quad Re < 1$$

$$C_D = \frac{24}{Re} \left(1 + \frac{Re^{2/3}}{6} \right) \quad , \quad 1 < Re < 1000 \quad (B-11)$$

$$C_D = 0.5 \quad , \quad 1000 < Re < 2 \times 10^5$$

Results

Equations (B-10) and (B-11) were programmed in an Excel workbook, Bubble Trajectory.xls. A $\Delta \hat{t}$ of 0.0001 was chosen and the resulting non-dimensional quantities converted back to dimensional quantities using the scaling parameters in Equations (B-6) and (B-7). The resulting time step was 2.54×10^{-6} sec.

The manifold velocity, u_o , was taken to be 5 kts = 8.44 fps. The air exit velocity, w_o , was arbitrarily taken to be 100 fps.

Displacements and velocity in the x-direction as a function of time are shown in Figure B - 1. Note that the velocity in the x-direction is essentially zero in less than 0.01 seconds and the displacement in the x-direction remains constant thereafter. In 0.01 seconds, the manifold has moved 0.084 feet.

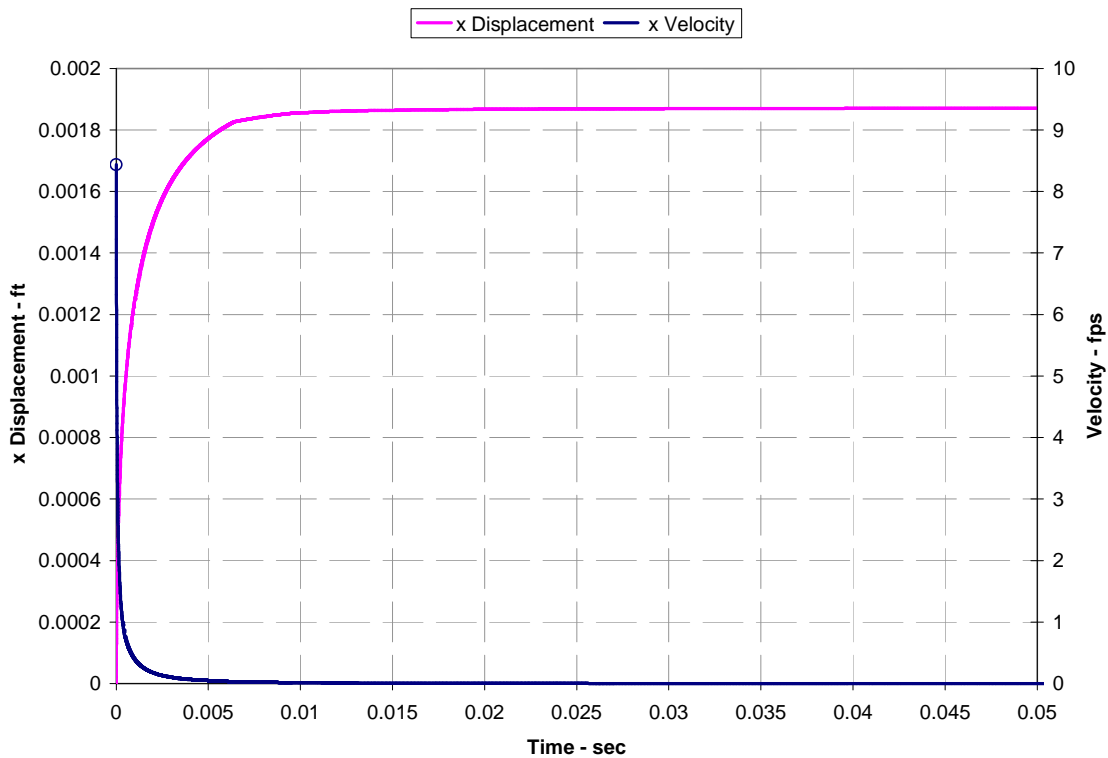


Figure B - 1 Displacement and Velocity in the x Direction

Displacements and velocity in the x-direction as a function of time are shown in Figure B - 2.

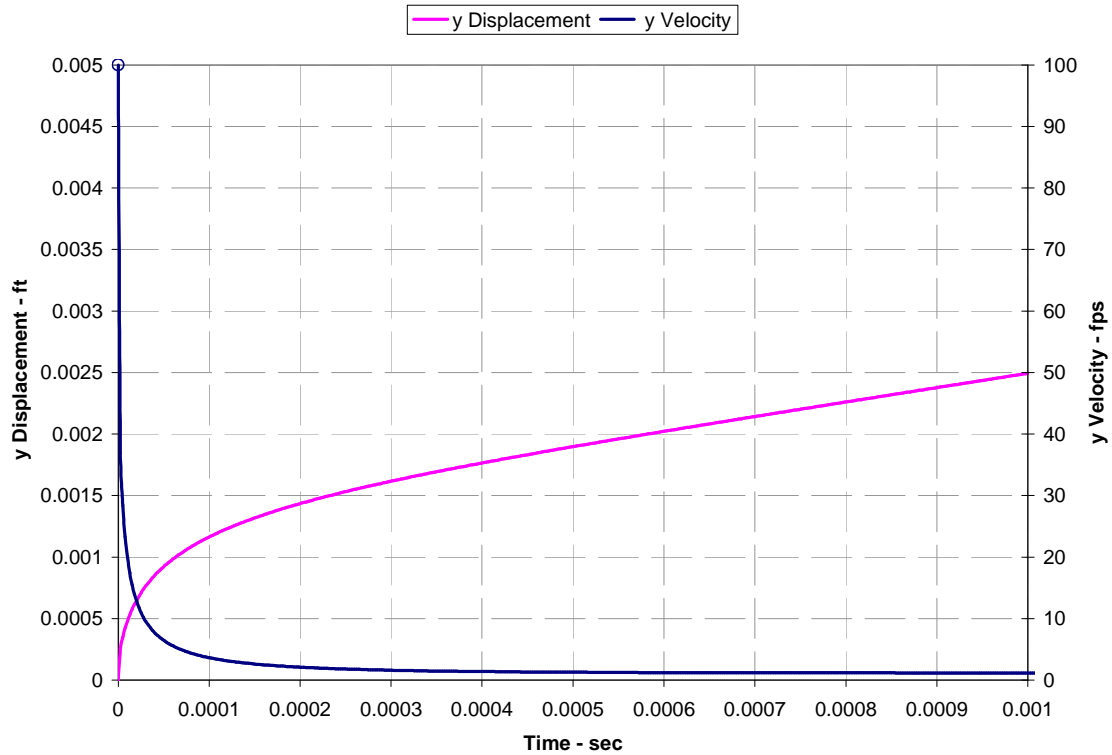


Figure B - 2 Velocity and Displacement in the y-Direction

Note that the initial velocity in the y-direction of 100 fps has decreased to what appears to be a constant value in 0.0004 seconds. At this time, the y displacement is 0.0018 ft. Actually, the y velocity continues to decrease and eventually reaches a constant value of 1.15 fps at 0.002 seconds, at which time the y displacement is 0.0037 ft. The value of 1.15 fps agrees well with bubble terminal rise velocities of about 30 - 33 cm/sec = 0.98 - 1.1 fps quoted in the literature.

Using time as a parametric value, the bubble trajectory may be plotted as shown in Figure B - 3.

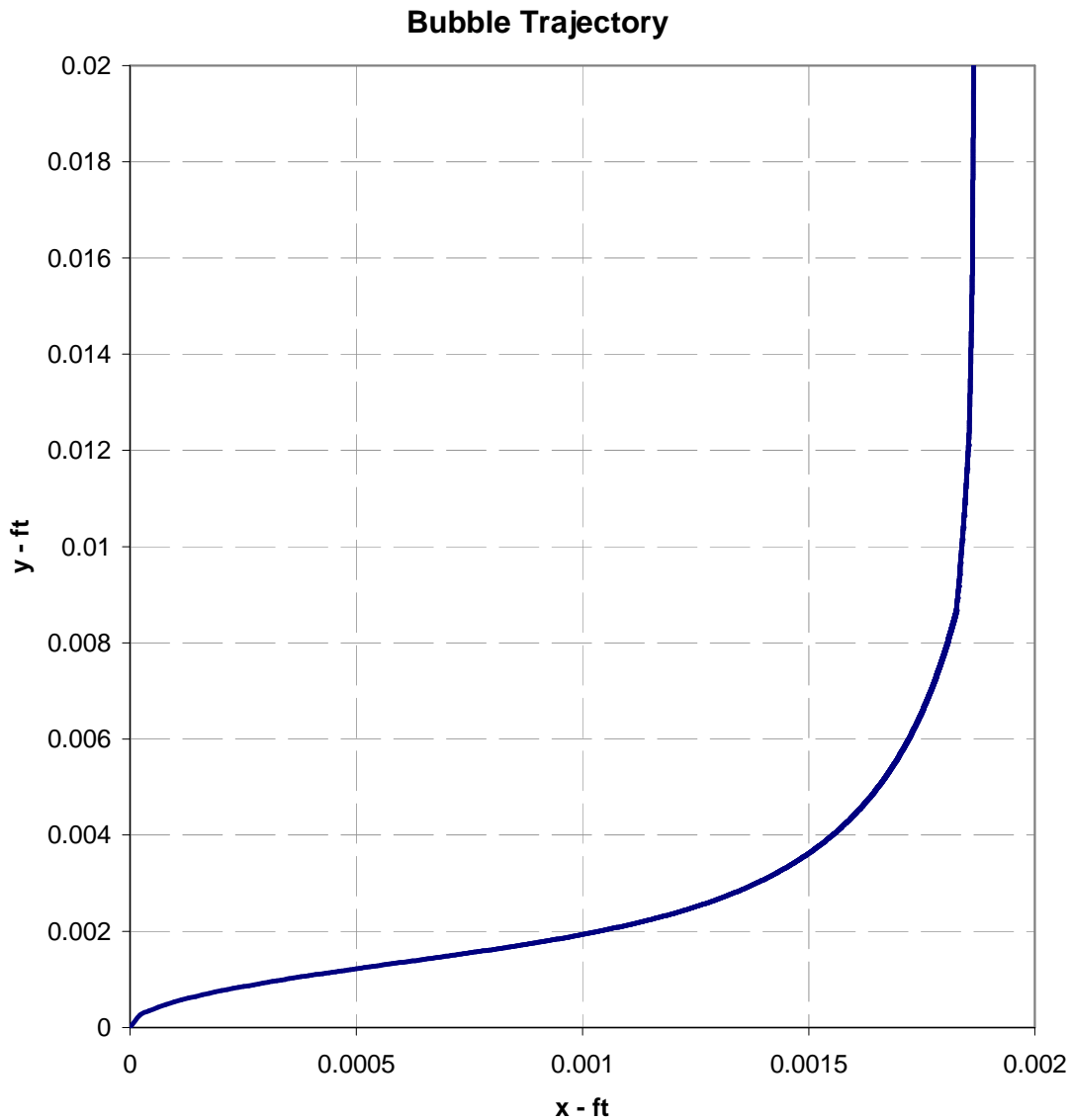


Figure B - 3 Bubble Trajectory

This plot shows that the bubble moves less than 0.002 ft in the direction of manifold travel. At the same time, the bubble has risen about 0.02 feet above the manifold nozzle exit.

The results shown in this bubble trajectory confirm that the motion of a manifold moving at a velocity of 5 kts may be neglected.

Appendix C

Excel Workbook Air Curtain Design.xls

Appendix C

Excel Workbook Air Curtain Design.xls

This workbook consists of four worksheets and three chart sheets containing plots of the data in the fourth worksheet. Each of the sheets is described on the following pages.

In addition, Visual Basic for Applications (VBA) code is contained in the usual Excel objects and in three modules. Documentation is contained in the comments in the code.

This workbook evolved over the course of this investigation. The emphasis has been on developing the correct method to evaluate the feasibility of the air bubble curtain. Therefore, this workbook contains vestiges of previous methods deemed unsuitable or inefficient. It is NOT user friendly, and is not necessarily the most efficient arrangement of the calculations described below. However, it is reasonably efficient, so no further work was done to improve either the efficiency or the user friendliness.

Numerical values and plots shown in the following figures are for the selected “best” design, Solution #58 of Appendix E.

AIR CURTAIN DESIGN		Created: Warren T. Jones, Ph.D.	10/3/08 4:05 PM
Input		Last Revision: 11/30/08 3:07 PM	
Properties of Air			
	Atmospheric pressure [Patm]	14.7	psi = 2116.8 lb/ft ²
	Gas Constant [GCR]	53.36	ft-lb/lbm-°R
	Specific Heat Ratio [k]	1.4	
Standard Conditions	Temperature [Tstd]	68	°F = 527.69 °R
	Pressure [Pstd]	14.7	psi = 2116.8 lb/ft ²
Sutherland's Formula	To [RefT]	524.07	°R
	C [SutherlancConst]	120	
	a[aFactor]	410.8589	
	b[bFactor]	397.328	
	m ₀ [muo]	0.01827	cp
Properties of Water			
	Density of water [rhow]	64	lbm/ft ³
	Compressibility of water [Betaw]	2.10E-08	ft ² /lb
	Seawater Temperature [Tsw]	40	°F = 499.69 °R
Gravity, Nozzle, and Plume Properties			
	Acceleration of gravity [g]	32.1739	ft/sec ²
	Sub-sonic Nozzle Coefficient [cdss]	0.65	
	Sonic Nozzle Coefficient [cds]	0.65	
	2-D Entrainment factor [EntFac]	0.103	
	2-D Velocity spreading factor [VelSpreadFac]	0.116	
	Ratio concentration to velocity width [lambda]	1.35	
	Lagrangian Spreading Coefficient [Lbeta]	0.145	
Design of Air Curtain			
	Vessel Speed [Vv]	5	kts = 8.445 fps
	Array Length [Larray]	50	ft
	Excess Length [L excess]	20	ft
	Depth of Manifold [H]	60	ft
	Maximum Number of Nozzles/ft [Maxn]	3	
	Maximum Nozzle dia [Maxd]	0.125	in = 0.010417 ft
	Max Speed of Sound Ratio [Maxcocw]	0.07	
	Minimum Pressure Drop Ratio in Manifold [PendoPinAllow]	0.98	
	Minimum Pressure Differential at Manifold End [PendDiffAllow]	2	psi
Calculated Quantities			
	Water Pressure at manifold [Po]	5956.8	psfa = 41.366667 psia
	Speed of Sound in water [cw]	4895.305798	fps
	Specific Impedance of water [Speclmp_w]	9737.693318	lb-sec/ft ³ = 1.530E+06 N-sec/m ³ = 1.530E+06 rayls
	Critical Pressure Ratio [rpc]	0.528281788	
	Max Pm for sonic velocity at nozzle [Pmmax]	11275.80041	psf = 78.30417 psi
	k/(k-1) [kokm1]	3.5	
	k/(k+1) [kokp1]	0.583333333	
	(k-1)/k [km1ok]	0.285714286	
	(k+1)/k [kp1ok]	1.714285714	
	(k+1)/(k-1) [kp1okm1]	6	
	Viscosity of air [mu_cp]	0.017589323	cp
	Viscosity [VisAir]	3.676E-07	lb-sec/ft ²
Plot Parameters			
	Number of Plot Points [NumPlotPts]	20	
	Number of integration steps [NumSteps]	20000	
	Number of output steps [NumOut]	1000	

Figure C - 1 Sheet "Input"

Sheet “Input”

This sheet is shown in Figure C - 1. Input quantities are arranged in groups. Properties of air and water are input in the first two groups. Gravity, Nozzle and Plume properties are input in the third group. Design variables are in the fourth group. Calculated quantities which do not depend on anything but these input values are shown next. At the bottom of the sheet, the group “Plot Parameters” contains values for the numerical integration of the simultaneous differential equations and the plots in the three chart sheets.

Input supplied by the user is shown in the yellow cells outlined in blue. An identifying label is shown to the left of each input cell along with the Excel name for that cell enclosed in square brackets. The values shown in these yellow cells were used throughout this investigation. The orange cells in the “Design of Air Curtain” group are those variables which were varied to produce the matrix of solutions described below under Sheet “SolutionSummary”

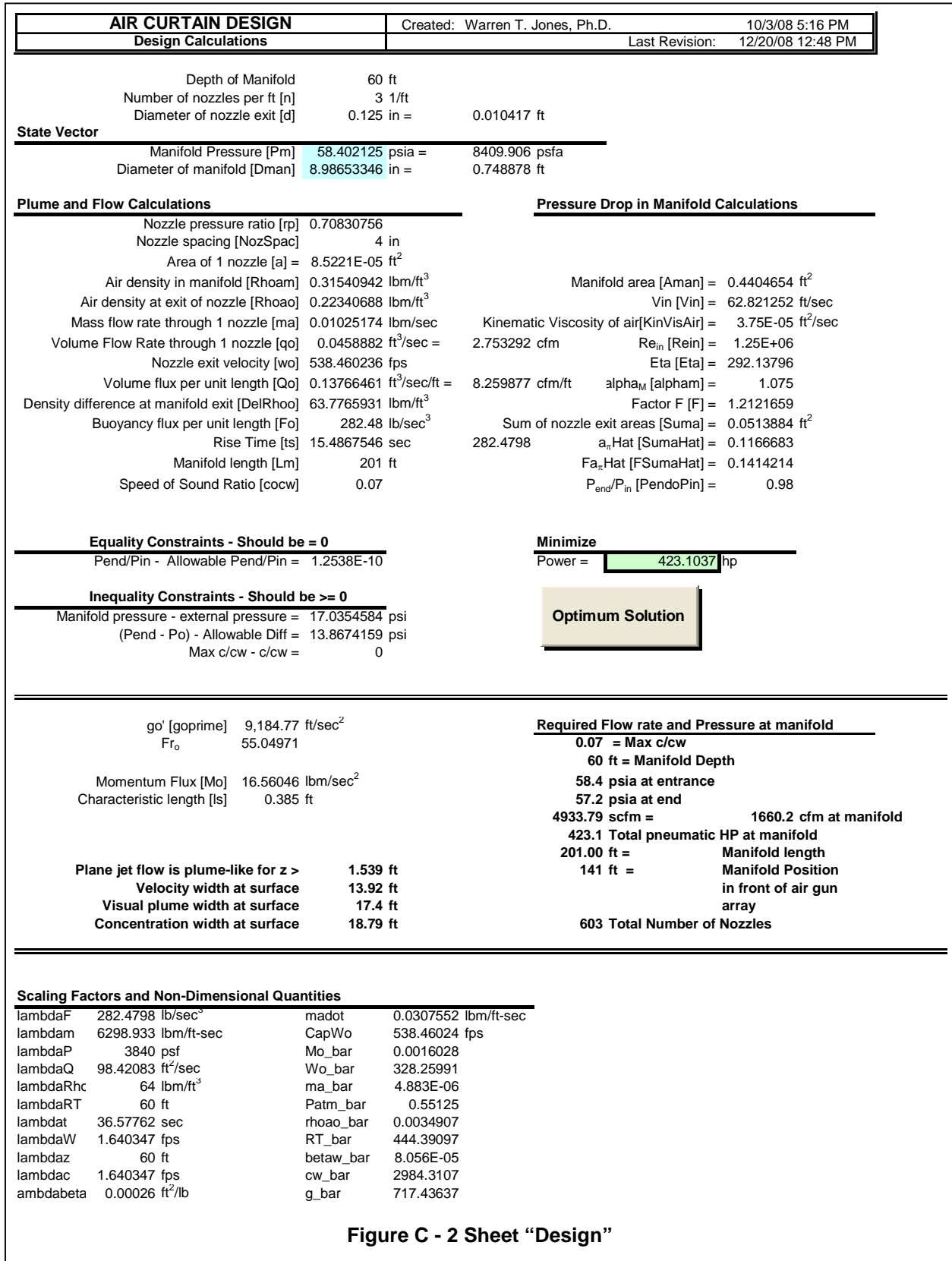


Figure C - 2 Sheet "Design"

Sheet “Design”

Sheet Description

This sheet is shown in Figure C - 2. All calculations for the design are done from this sheet. Bold headings separate various regions. The State Vector is shown at the top, with a light blue background for the cells. The Solver Add-In varies the values in these cells in order to satisfy the constraints and minimize the power shown in the light green cell on the right.

Immediately below the State Vector are the Plume and Flow Calculations, and to their right are the Pressure Drop in the Manifold Calculations. Equality and Inequality Constraints are shown below the Plume and Flow Calculations.

Various quantities of interest in evaluating optimal designs based on the Input in Figure C - 1 are listed between the two double lines in bold print. In normal print are quantities of general fluid dynamics interest which do not necessarily enter into an evaluation of the suitability of this design. One item of both optimal design interest and fluid dynamics interest is the height above which the flow is plume-like. The topmost bold item on the left side of the page below the first double line is “Plane jet flow is plume-like for $z > 2.788$ ft.” That means that for all heights above the manifold greater than about 2-3/4 ft, the flow in the bubble curtain is driven solely by buoyancy.

Scaling factors for the non-dimensionalization of the differential equations are shown below the second double line. Also shown there are values of various non-dimensional quantities used in the solution of the differential equations.

Two buttons are also located on this page with captions of “Update Plots” and “Optimum Solution.” The “Update Plots” button calculates and updates the table on Sheet “PlotData” which is used to create the charts contained in the last three sheets of the workbook: “cht_s”, “cht_cRatio”, and “cht_lratio.” The “Optimum Solution” button is used to initiate execution of the VBA routines used in obtaining an optimum solution.

Calculation Algorithms

For any value of manifold pressure, P_m , in the State Vector, the following algorithm is used to calculate the cells under the heading “Plume and Flow Calculations”

- The nozzle pressure ratio, r_p , is calculated from Equation (52) on page 15.
- The nozzle spacing is calculated from Equation (12) on page 8. (This step is not necessary for the following steps – it’s included just for easy reference.)
- The area of one nozzle, a , is calculated from $\pi d^2/4$
- Air density in the manifold, ρ_{aM} , is calculated from Equation (58) on page 16.
- Since the “nozzles” in the manifold will likely be just holes, they are treated as orifices. So air density at the exit of the nozzle, ρ_{ao} , is calculated from the perfect gas relationship and the pressure and temperature in the water at the manifold depth.
- If $r_p > r_{pc}$ as given by Equation (54) on page 15, then the subsonic mass flow rate is calculated from Equation (51) on page 15; otherwise the sonic mass flow rate is calculated from Equation (55) on page 16.
- The flow rate through one nozzle, q_o , is calculated by Equation (56) on page 16.
- The nozzle exit velocity, w_o , is calculated from Equation (57) on page 16.
- The volume flux per unit length, Q_o , is calculated from Equation (11) on page 7.
- The density difference at the manifold exit is simply the water density, ρ_w , minus the air density at the nozzle exit, ρ_{ao} .

- Buoyancy flux per unit length at the nozzle exit, F_o , is calculated from the right-hand equality in Equation (19) on page 9 using the air density at the nozzle exit, ρ_{ao} .
- The rise time, t_s , is the value calculated in the table on Sheet “PlotData” (shown with an orange background in Figure C - 4).
- The manifold length, L_M , is calculated from Equations (68) through (71) on page 19.
- The Speed of Sound Ratio is the maximum value of c/c_w and is calculated by the User Function MaxSpeed2 (described below)
- The objective function is the pneumatic horsepower given by Equation (73) on page 21.

The calculations just described only involve the first variable in the State Vector, P_m . However, several quantities calculated above are also involved in calculating the Pressure Drop Ratio in the manifold, namely a , ρ_{aM} , Q_o , and L_M . For any value of manifold diameter, D_{Man} , in the State Vector, the following algorithm is used to calculate the cells under the heading “Pressure Drop in Manifold Calculations”

- The manifold area, A_{man} , is calculated from $\pi D^2/4$.
- The velocity entering the manifold V_{in} , is calculated from $Q_o L_M / A_{man}$
- Kinematic viscosity of the air in the manifold is given by Equations (60) and (61) on page 17
- Calculation of the remaining quantities ending with P_{end}/P_{in} follow Equations (62) through (67).

Button “Update Plots”

Clicking this button executes the VBA subroutine SolveSys(bWRITE As Boolean) with bWRITE set equal to TRUE. This subroutine reads the required non-dimensional values currently in Sheets “Design” and “Input” and calls the Runga-Kutta integration routine, RKsys2. Because the argument bWRITE is TRUE, the table on Sheet “PlotData” is updated during the course of numerical integration.

User Function MaxSpeed2

This function calculates the maximum value of the speed of sound ratio, c/c_w , occurring from the manifold to the surface. To do this, it calls the VBA subroutine SolveSys(bWRITE As Boolean) with bWRITE set equal to FALSE. With bWRITE = FALSE, nothing is written out. This is a necessary requirement, because user functions cannot modify the contents of any cell except the cell in which the call to the user function is located. This function returns the maximum value of c/c_w for use in the third constraint shown in Equation (75) on page 21. In order to ensure that this function is evaluated every time the Solver add-in changes the values in the State Vector, this user function has arguments P_M and D_{Man} . So whenever the Solver add-in varies values in the State Vector, this function is recalculated.

Button “Optimum Solution”

The following algorithm is executed by clicking on the “Optimum Solution” button.

1. Begin an iteration loop
2. Execute the Solver. The Solver varies the State Vector to determine the values which minimize the pneumatic hp. During these calculations, the rise time, t_s , has a value equal to that in the table on Sheet “PlotData”
3. Recalculate the rise time by calling SolveSys(TRUE). This updates the table on Sheet “PlotData” and the rise time on Sheet “Design” is equal to the rise time calculated in this table.
4. If the new rise time differs from the old rise time by less than some value (selected to be 10^{-8} in this case), exit the loop.
5. Go to step 1.

Because the majority of the bubble curtain is driven by buoyancy, the rise time does not vary very much, even with large changes in manifold pressure, P_M . Therefore, this iteration scheme converges very rapidly. Most solutions were obtained on the second pass, and none required more than three passes.

Sheet “SolutionSummary”

This sheet contains the matrix of solutions discussed in the body of this report. Values of key items from Sheet “Design” for each solution have been copied and pasted into this sheet. No calculations are done in this sheet; it is simply a storage place for the various solutions. Details of the sheet can be seen in Appendix E.

Sheet “PlotData”

This sheet contains data to be plotted in the chart sheets. This data is obtained through the non-dimensional solution of the simultaneous, non-dimensional differential equations and through calculations made on this sheet. These calculations are arranged in one table which is too large to print out onto a single sheet of paper, so it is described in the following figures.

i	Non-Dimensional Integration				Non-Dimensional Calculated		
	zi_bar	Mi_bar	mi_bar	t_bar	Wi_bar	rhoai_bar	si_bar
0	0	0.001603	4.88261E-06	0	328.2599	0.003491	1
1	0.05	0.025141	0.011690211	0.023176517	2.150585	0.003378	0.1100723
2	0.1	0.049472	0.022811926	0.046329558	2.168684	0.003266	0.0615219
3	0.15	0.074442	0.034029024	0.069285729	2.1876	0.003153	0.0435297
4	0.2	0.100092	0.04534557	0.092040173	2.207313	0.003041	0.0342041
5	0.25	0.126467	0.056765807	0.114588028	2.227879	0.002928	0.0285386
6	0.3	0.153619	0.068294303	0.136924157	2.249367	0.002816	0.0247645
7	0.35	0.181603	0.079936006	0.159043097	2.271857	0.002703	0.0220985
8	0.4	0.210483	0.091696296	0.18093901	2.295436	0.002591	0.0201411
9	0.45	0.240329	0.103581041	0.202605649	2.320207	0.002478	0.0186676
10	0.5	0.271223	0.115596667	0.224036298	2.346284	0.002366	0.0175428
11	0.55	0.303254	0.12775024	0.245223723	2.373802	0.002253	0.0166811
12	0.6	0.336527	0.140049562	0.266160096	2.402913	0.002141	0.0160265
13	0.65	0.371162	0.152503291	0.286836916	2.433798	0.002028	0.0155419
14	0.7	0.407299	0.165121083	0.307244912	2.466666	0.001916	0.0152026
15	0.75	0.445099	0.177913779	0.327373921	2.501767	0.001803	0.0149931
16	0.8	0.484755	0.190893621	0.347212743	2.539399	0.001691	0.0149049
17	0.85	0.526497	0.204074545	0.36674896	2.579923	0.001578	0.0149359
18	0.9	0.5706	0.217472541	0.385968707	2.623781	0.001465	0.0150894
19	0.95	0.617405	0.231106142	0.404856378	2.671522	0.001353	0.0153755
20	1	0.667333	0.244997062	0.423394248	2.72384	0.00124	0.0158123

Figure C - 3 Non-Dimensional Quantities

Figure C - 3 shows the non-dimensional quantities. The columns under the “Non-Dimensional Integration” heading are written by the Subroutine SolveSys() described above. The columns under the “Non-Dimensional Calculated” heading are calculated on this sheet using Equations (36), (30), and (38) on pages 12 and 13 of the body of this report.

Figure C - 4 shows the dimensional quantities calculated using the scaling factors in Equations (24) and (25) on page 11 of the body of this report. The cell highlighted in orange is the dimensional value of rise time which is referenced on the Sheet “Design” and used in the iteration loop under the heading ‘Button “Optimum Solution”’ above.

Figure C - 5 shows the calculations of the speed of sound and specific acoustic impedance ratios using the second equality in Equation (21) on page 10 and Equations (6), (8), and (10) on pages 6 and 7.

Dimensional							
i	z (ft)	M (lbm/sec ²)	m (lbm/ft-sec)	t (sec)	W (ft/sec)	rhoa (lbm/ft ³)	s (-)
0	0	993.62779	0.0307552	0	538.46023	0.2234069	1
1	3	15585.939	73.635863	0.8477419	3.5277057	0.216206	0.110072
2	6	30669.894	143.6908	1.6946251	3.5573949	0.2090051	0.061522
3	9	46149.97	214.34655	2.5343072	3.5884234	0.2018043	0.043530
4	12	62051.566	285.62872	3.3666106	3.620759	0.1946034	0.034204
5	15	78402.948	357.56403	4.1913575	3.6544945	0.1874025	0.028539
6	18	95235.5	430.18126	5.00836	3.6897431	0.1802017	0.024764
7	21	112584.19	503.51157	5.8174182	3.7266335	0.1730008	0.022099
8	24	130488.13	577.58885	6.6183187	3.765312	0.1657999	0.020141
9	27	148991.33	652.45007	7.4108328	3.8059446	0.1585991	0.018668
10	30	168143.47	728.1357	8.194715	3.848721	0.1513982	0.017543
11	33	188001.04	804.69024	8.9697006	3.8938595	0.1441973	0.016681
12	36	208628.64	882.16285	9.7355033	3.9416123	0.1369965	0.016027
13	39	230100.61	960.60806	10.491812	3.9922736	0.1297956	0.015542
14	42	252503.21	1040.0867	11.238288	4.0461884	0.1225947	0.015203
15	45	275937.31	1120.667	11.974559	4.1037659	0.1153939	0.014993
16	48	300522.05	1202.4262	12.700216	4.1654954	0.108193	0.014905
17	51	326399.55	1285.4519	13.414805	4.2319687	0.1009922	0.014936
18	54	353741.47	1369.845	14.117817	4.3039111	0.0937913	0.015089
19	57	382757.99	1455.7222	14.808683	4.3822234	0.0865904	0.015376
20	60	413710.54	1543.2202	15.486755	4.4680441	0.0793896	0.015812

Figure C - 4 Dimensional Quantities

Additional Calculated Values						
i	P lb/ft ²	Air bubble Compres- sibility ft ² /lb	Speed of Sound, c ft/sec	Speed of Sound Ratio, c/c _w -	Specific Acoustic Impedanc e, I lb-sec/ft ³	Specific Acoustic Impedanc e Ratio, I/I _w -
0	5956.8	1.68E-04				
1	5764.8	1.73E-04	171.88373	0.0351119	304.4018	0.03126
2	5572.8	1.79E-04	220.05851	0.044953	410.8956	0.042196
3	5380.8	1.86E-04	254.5585	0.0520005	484.3928	0.049744
4	5188.8	1.93E-04	280.55861	0.0573118	539.0536	0.055357
5	4996.8	2.00E-04	300.46005	0.0613772	580.6654	0.059631
6	4804.8	2.08E-04	315.61271	0.0644725	612.3099	0.06288
7	4612.8	2.17E-04	326.86925	0.066772	635.8753	0.0653
8	4420.8	2.26E-04	334.81144	0.0683944	652.6243	0.06702
9	4228.8	2.36E-04	339.85845	0.0694254	663.4542	0.068133
10	4036.8	2.48E-04	342.32467	0.0699292	669.0313	0.068705
11	3844.8	2.60E-04	342.4533	0.0699554	669.8671	0.068791
12	3652.8	2.74E-04	340.43699	0.0695436	666.364	0.068431
13	3460.8	2.89E-04	336.43129	0.0687253	658.8458	0.067659
14	3268.8	3.06E-04	330.56369	0.0675267	647.5766	0.066502
15	3076.8	3.25E-04	322.93991	0.0659693	632.7748	0.064982
16	2884.8	3.47E-04	313.64842	0.0640713	614.6227	0.063118
17	2692.8	3.71E-04	302.76372	0.0618478	593.2736	0.060925
18	2500.8	4.00E-04	290.34879	0.0593117	568.8567	0.058418
19	2308.8	4.33E-04	276.45695	0.0564739	541.4814	0.055607
20	2116.8	4.72E-04	261.13316	0.0533436	511.2401	0.052501

Figure C - 5 Ratios

Some other data appear on this sheet which have no significance as far as evaluating the feasibility of the air curtain, and so they are not shown here. One set of data does deserve mention, however. Using one particular set of input data, the non-dimensional differential equations were integrated numerically with different number of steps, and the solutions compared. Eventually, 20,000 steps were chosen. The non-dimensional values obtained by doubling the number of steps to 40,000 were the same to 3 significant figures. Values obtained with 80,000 steps were the same as obtained with 40,000 steps to 4 significant figure. Since solution times increased with the number of steps, 20,000 steps seemed to be a reasonable compromise between accuracy and solution time.

Sheet "cht_s"

The values of z and s shown in Figure C - 4 are plotted on this sheet. Significance of this plot is discussed in the body of the report.

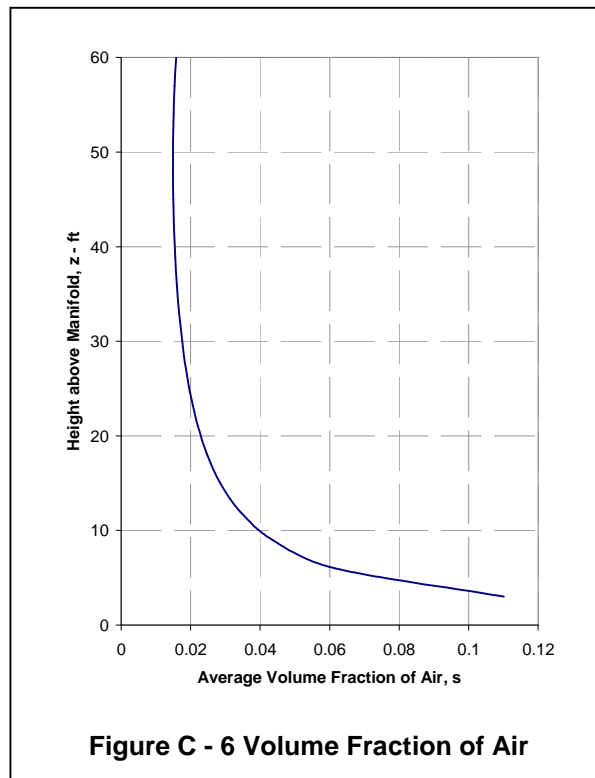
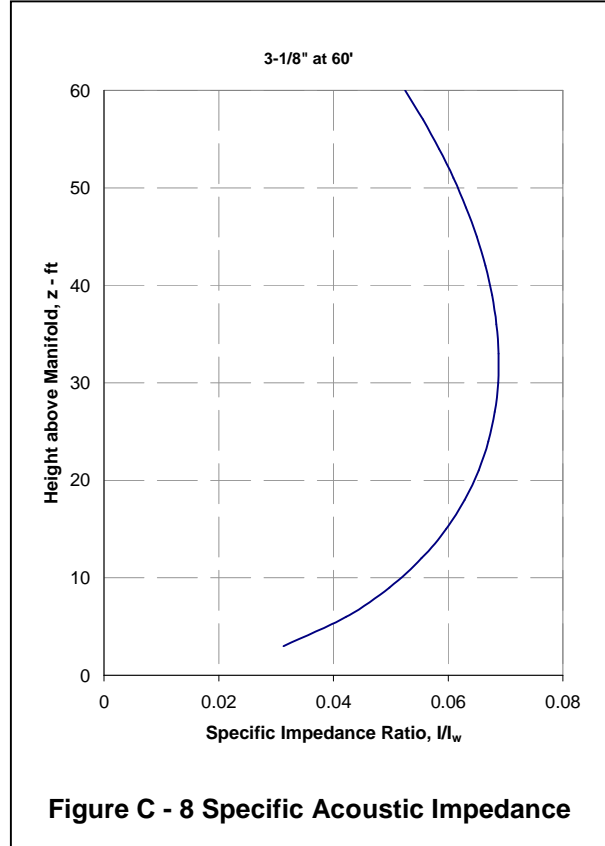
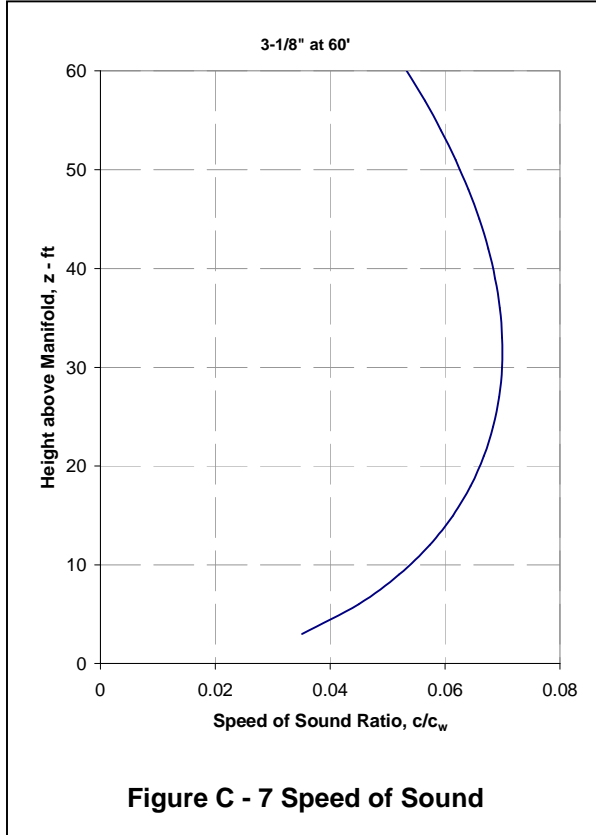


Figure C - 6 Volume Fraction of Air

Sheets “cht_cRatio” and “cht_lratio”

These two sheets plot the speed of sound ratio, c/c_w , and the specific acoustic impedance ratio, I/I_w , [shown in Figure C - 5] as a function of height above the manifold, z . Significance of these plots is discussed in the body of the report.



Note that the Specific Acoustic Impedance curve looks almost identical to the Speed of Sound curve. In fact, it varies slightly from the c/c_w curve.

Specific impedance I is defined as $I = c\rho$, so

$$\frac{I}{I_w} = \frac{\rho}{\rho_w} \frac{c}{c_w}$$

Examination of the complete data set shown in Figure C - 5 shows that $\frac{\rho}{\rho_w} = \frac{I/I_w}{c/c_w}$ varies from 0.894 at

$z = 3$ ft to 0.984 at $z = 60$ ft. Thus the Specific Acoustic Impedance curve is the Speed of Sound curve multiplied by a number varying from about 0.9 to 0.98. Therefore, the shape of the curves in the above two figures are similar, and the casual observer will not notice any difference in the numerical values plotted.

Appendix D

Comparison with Experiments

Appendix D

Comparison with Experiments

Sixma and Stubbs (1996) of Shell Venezuela and Western Geophysical investigated shot generated noise observed in Lake Maracaibo and the use of bubble screens to suppress unwanted noise and reflections peculiar to that region. As a precursor to the field test, Western Geophysical conducted tests to determine the attenuation properties of a bubble screen. Thanks to Shell Oil USA, the Western Geophysical report to Shell Venezuela, Anonymous (1996), has been made available to the present investigation.

The tests were conducted in Western Geophysical's test site near Houston in a 25-foot deep pit with a manifold on bottom located between an air gun and a hydrophone, each at 12 feet above bottom. Waveforms, amplitude spectra, and attenuation spectra are presented in the report for various combinations of orifice size and air supply pressure and flow rate. Percent air saturation is quoted, but no mention is made of how it was determined.

Equations presented in the section, "Compressible Fluid Flow Through the Nozzles" on page 15 in the body of this report were copied from the workbook Air Curtain Design.xls into a new Excel workbook along with pertinent input quantities. The resulting worksheet to calculate flow rates based on supply pressure is shown in Figure D- 1.

Input quantities which were explicitly stated in the Western Geophysical report are shown with a yellow background; those cells containing assumed values are shown with an orange background. For example, it is assumed that the pit was filled with fresh water at 85 °F. In the Comparison table at the bottom of the figure, the supply pressures and flow rates quoted in the Western Geophysical report are shown with a yellow background.

The remaining cells in the Comparison table contain the formulas for calculating compressible flow through nozzles for the three orifice sizes used in the Western Geophysical tests.

No description is given of the shape of the nozzles used. As shown in J. E. Gasho & Associates (unknown), the discharge coefficients can have a wide range of values, depending on the nozzle shape. So for a first approximation, both the subsonic and sonic discharge coefficients were taken to be 1.0.

AIR CURTAIN DESIGN COMPARISON												Created: Warren T. Jones, Ph.D 10/25/08 11:41 AM	
Western Geophysical												Last Revision: 11/14/08 2:05 PM	
Properties of Air						Properties of Water							
Atmospheric pressure [Patm]		14.7		psi = 2116.8 lb/ft ²		Density of water [rho]		62.4		lbm/ft ³			
Gas Constant [GCR]		53.36		ft-lb/lbm-°R		Compressibility of water [Betaw]		2.10E-08		ft ² /lb			
Specific Heat Ratio [k]		1.4				Seawater Temperature [Tsw]		85		°F = 544.69 °R			
Standard Temperature [Tstd]		68		°F = 527.69 °R									
Conditions Pressure [Pstd]		14.7		psi = 2116.8 lb/ft ²									
Gravity and Plume Properties						Design of Air Curtain							
Acceleration of gravity [g]		32.1739		ft/sec ²		Depth of Manifold [H]		25		ft			
Sub-sonic Nozzle Coefficient [cdss]		1				Number of Nozzles per ft [n]		3		1/ft			
Sonic Nozzle Coefficient [cds]		1				Length of Manifold [LM]		33		ft			
Calculated Quantities													
Water Pressure at manifold [Po]		3676.8		psfa = 25.53333 psia									
Critical Pressure Ratio [rpc]		0.528282											
Max Pm for sonic velocity at nozzle [Pmmax]		6959.922		psf = 48.33279 psi									
k/(k-1) [kokm1]		3.5											
(k+1)/k [kp1ok]		1.714286											
(k+1)/(k-1) [kp1okm1]		6											
Comparison													
Western Geophysical Data - Table 1 p. 10													
Pm	P	Q	Nozzle pressure ratio [rp]	Air density in manifold [Rhoam]	Air density at exit of nozzle [Rhoao]	Mass Flow rate [m]	Volume Flow Rate through 1 nozzle [qo]	Nozzle exit velocity [wo]	Volume flux per unit length [Qo]	Total Flow Rate	Total Flow Rate	Ratio Meas/Calc	
psfa	psia	scfm	-	lb _m /ft ³	lb _m /ft ³	lbm/sec	ft ³ /sec	fps	cfm/ft	cfm	scfm	-	
1/64 Orifice = 0.015625 in = 0.001302 ft area = 1.33E-06 ft ²													
4464	31	7	0.823656	0.153589	0.133714	0.000106	0.000791	594.1043	0.142398	4.69912	7.907445	0.885242	
6480	45	13	0.567407	0.222951	0.148738	0.000196	0.001317	989.1809	0.237091	7.824014	13.16586	0.987402	
7920	55	16	0.464242	0.272496	0.157515	0.00024	0.001525	1145.498	0.274558	9.060414	15.24641	1.049427	
8928	62	18	0.411828	0.307177	0.162999	0.000271	0.001662	1247.837	0.299087	9.869874	16.60853	1.08378	
13824	96	25	0.265972	0.475629	0.184687	0.000419	0.002271	1705.242	0.40872	13.48776	22.69653	1.10149	
3/64 Orifice = 0.046875 in = 0.003906 ft area = 1.2E-05 ft ²													
4752	33	74	0.773737	0.163498	0.136124	0.00111	0.008151	680.148	1.467188	48.41722	81.47408	0.908264	
6192	43	113	0.593798	0.213042	0.146818	0.001674	0.011405	951.678	2.052922	67.74643	114.0003	0.991225	
7632	53	141	0.481761	0.262587	0.155856	0.002084	0.013369	1115.587	2.406501	79.41453	133.6348	1.055114	
9072	63	165	0.405291	0.312132	0.163746	0.002477	0.015126	1262.18	2.722724	89.8499	151.1949	1.091306	
10368	72	184	0.35463	0.356722	0.170114	0.002831	0.01664	1388.494	2.995204	98.84175	166.326	1.106261	
3/32 Orifice = 0.09375 in = 0.007813 ft area = 4.79E-05 ft ²													
4320	30	228	0.851111	0.148634	0.132467	0.003447	0.026022	542.8341	4.683921	154.5694	260.1017	0.87658	
4752	33	295	0.773737	0.163498	0.136124	0.004438	0.032604	680.148	5.868754	193.6689	325.8963	0.905196	

Figure D- 1 - Excel Workbook for Calculating Flowrates

The last column in the Comparison table shows the ratio of the measured flow rate to the calculated flow rate. This ratio is in fact the definition of the discharge coefficient for a nozzle, so if discharge coefficients of 1.0 are used in the calculations, this column gives the value of discharge coefficient which would result in the calculated flow matching the measured flow exactly.

For each nozzle size, the lowest two pressures result in subsonic flows. The highest three pressures for the 1/64" and 3/64" are sonic. The table indicates a subsonic discharge coefficient of about 0.9⁺ and a sonic discharge coefficient of about 1.0⁺ would match the measured flow. These results were obtained by adjusting the length of the manifold. A length less than the 33 ft used here would result in both subsonic and sonic discharge coefficients being greater than 1.0, which is impossible.

The calculated flow rates using the new values of discharge coefficient and the measurements of flow rates presented in the Western Geophysical report are in general agreement as shown in Figure D- 2 and Figure D-3

In Figure D- 2, the solid curves are drawn through the measured flow rates as listed in Table 1 of the Western Geophysical report; the data points represent flow rates calculated from the workbook shown in

Figure D- 1. A direct comparison of the measured and calculated value for each value of supply pressure is shown in Figure D-3.

Agreement is excellent on the 1/64" nozzle. For the 3/64" nozzle, calculated results for the two highest pressures (and flow rates) fall below the measured values. The largest difference is with the 3/32" nozzle. Calculated flow rates for both values of pressure lie well above the measured values.

This discrepancy at high flow rates (with the largest nozzles) can be explained by the absence of pertinent information in the Western Geophysical report. The pressures stated in the report are undoubtedly supply pressures measured at the regulator on the bank of high pressure air bottles located on the pier. Nothing is stated about the size or length of the conduit for the air from this regulator to the manifold at the bottom of the pit.

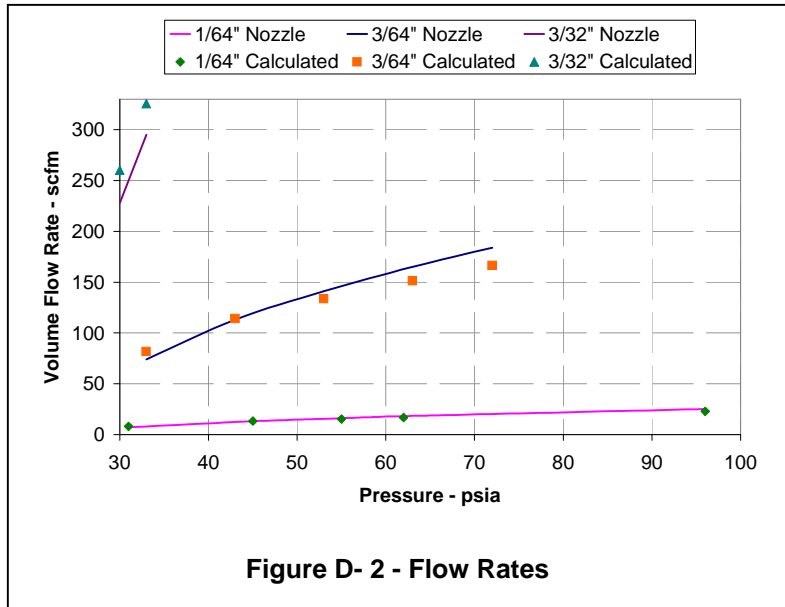


Figure D- 2 - Flow Rates

Consider the highest flow rate listed in Figure D- 1. Assuming the conduit is the same diameter as the manifold, 2", the pressure head loss in 26 ft of conduit would be about 1.5 psi for a flow rate of 295 scfm [see the friction loss nomograph in the J. E. Gasho web site, J. E. Gasho & Associates (unknown)]. Decreasing the manifold pressure from 33 to 31.5 psi results in a calculated flow rate of 295.8 scfm, an almost exact match for the measured value.

So if at least 26' of conduit existed between the supply and the manifold in 25' of water, then the highest calculated flow rate is not greater than the measured flow rate as indicated in Figure D- 2 and Figure D-3.

Of course, at lower flow rates, friction loss between the supply and the manifold would be less. So the supply pressure and manifold pressure would be closer in value, and smaller differences would exist between the measured flow rate and the value calculated using the supply pressure.

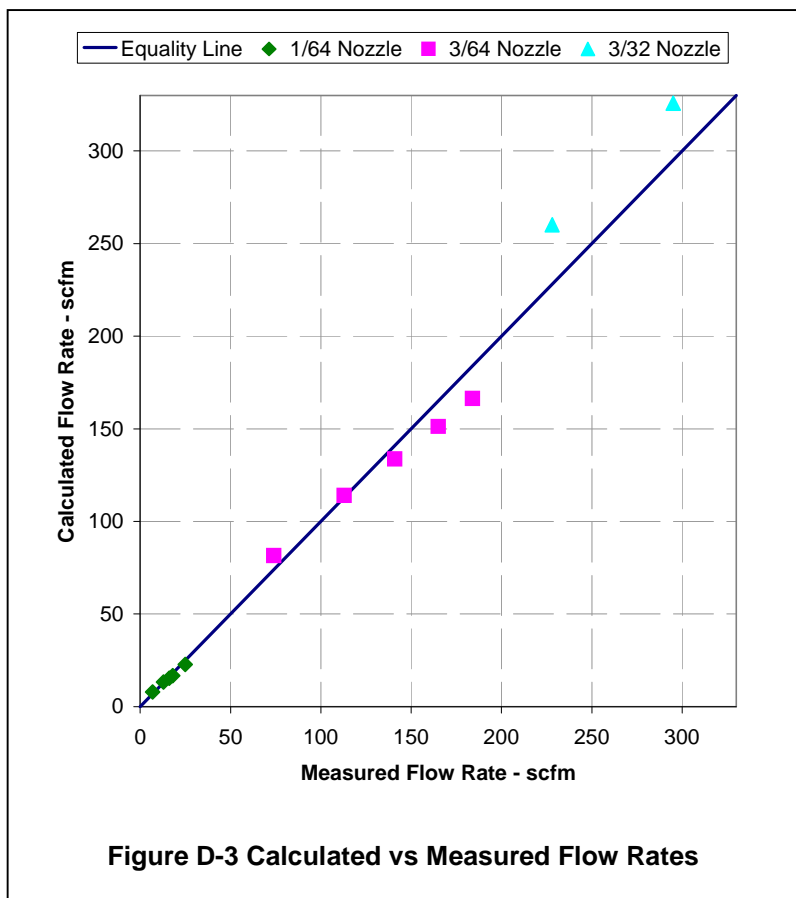


Figure D-3 Calculated vs Measured Flow Rates

Appendix E

Solution Matrix

The solution matrix contained in the Sheet "SolutionSummary" of the Air Curtain Design.xls workbook is shown on the following pages in Table E - 1 through Table E - 6. The headings on the columns are self-explanatory.

These tables are followed by plots of the pneumatic hp and manifold diameter vs. maximum c/cw ratio in Figure E - 1 through Figure E - 10.

Appendix E

Solution Matrix

Table E - 1

AIR CURTAIN DESIGN										Created: Warren T. Jones, Ph.D.		10/29/08 11:05 AM				
Solutions Summary										Last Revision: 12/19/08 9:42 AM						
Solution #	Max Speed of Sound Ratio c/c_w (-)	Non-Dim Height, z/H , at Max c/c_w (-)	Depth of Manifold [H] (ft)	Number of nozzles per ft [n] (1/ft)	Diameter of nozzle exit [d] (in)	Manifold Pressure [Pm] (psia)	Diameter of manifold [Dman] (in)	Pressure at Manifold End [Pend] (psia)	Flow Rate (scfm)	Total Pneumatic HP at manifold (hp)	Rise Time (sec)	Manifold length (ft)	Manifold Position in front of array (ft)	Total Number of Nozzles (-)	Pressure Diff at Manifold Beginning (psi)	Pressure Diff at Manifold End (psi)
1	0.0797597	0.503	70	3	0.1875	48.786848	14.331	47.8	5582.1	361.1	18.55	227	167	681	2.98	2.00
2	0.07	0.5009	70	3	0.1875	52.594654	13.67657	51.5	7662.8	534.4	16.18	207	147	621	6.78	5.73
3	0.06	0.49735	70	3	0.1875	64.207413	12.992926	62.9	11298.3	961.9	13.74	187	126	561	18.40	17.11
4	0.0727281	0.50185	70	4	0.1875	48.786848	16.022888	47.8	6983.8	451.8	16.85	213	152	852	2.98	2.00
5	0.07	0.50125	70	4	0.1875	49.599492	15.793269	48.6	7653.1	503.3	16.19	207	147	828	3.79	2.80
6	0.06	0.4979	70	4	0.1875	55.983493	15.004	54.9	11272.9	836.8	13.75	187	126	748	10.17	9.05
7	0.055	0.4953	70	4	0.1875	63.851954	14.553	62.6	14044.4	1189.0	12.52	176	116	704	18.04	16.76
8	0.0639201	0.49985	70	6	0.1875	48.786848	18.76923	47.8	9590.5	620.4	14.72	195	134	1170	2.98	2.00
9	0.06	0.49845	70	6	0.1875	50.272125	18.377257	49.3	11247.7	749.7	13.76	187	126	1122	4.46	3.46
10	0.05	0.4927	70	6	0.1875	60.576533	17.308923	59.4	18020.5	1447.4	11.30	166	105	996	14.77	13.55
11	0.1	0.5048	70	3	0.125	49.532974	10.396325	48.5	3273.8	215.0	23.44	268	208	804	3.72	2.73
12	0.09	0.5037	70	3	0.125	53.005561	9.990977	51.9	4200.6	295.2	21.01	248	187	744	7.19	6.13
13	0.08	0.50205	70	3	0.125	60.999265	9.5507946	59.8	5552.1	449.1	18.59	227	167	681	15.19	13.97
14	0.07	0.4994	70	3	0.125	82.161927	9.1145571	80.5	7711.6	840.1	16.14	207	146	621	36.35	34.71
15	0.065	0.4974	70	3	0.125	103.87529	8.8670597	101.8	9249.0	1273.9	14.91	196	136	588	58.06	55.99
16	0.0944345	0.5045	70	4	0.125	48.786848	11.750386	47.8	3745.1	242.3	22.09	257	197	1028	2.98	2.00
17	0.09	0.504	70	4	0.125	49.828018	11.538127	48.8	4195.5	277.2	21.02	248	188	992	4.02	3.02
18	0.08	0.5025	70	4	0.125	54.235309	11.054308	53.2	5566.6	400.3	18.60	228	167	912	8.42	7.34
19	0.07	0.5001	70	4	0.125	65.657642	10.526208	64.3	7689.5	669.4	16.16	207	146	828	19.85	18.53
20	0.065	0.4983	70	4	0.125	78.186911	10.26618	76.6	9261.0	960.1	14.94	197	136	788	32.38	30.81
21	0.06	0.49585	70	4	0.125	100.37384	9.9734426	98.4	11308.3	1505.0	13.70	186	126	744	54.56	52.56
22	0.082842	0.50335	70	6	0.125	48.786848	13.690965	47.8	5093.1	329.5	19.30	233	173	1398	2.98	2.00
23	0.08	0.5029	70	6	0.125	49.514405	13.540545	48.5	5556.6	364.8	18.61	228	167	1368	3.70	2.71
24	0.075	0.502	70	6	0.125	51.371747	13.205578	50.3	6471.0	440.8	17.40	217	157	1302	5.56	4.53
25	0.07	0.50075	70	6	0.125	54.431991	12.893972	53.3	7667.6	553.4	16.18	207	147	1242	8.62	7.53
26	0.0755553	0.51505	65	3	0.1875	46.519274	13.979654	45.6	5141.2	333.3	17.19	216	155	648	2.93	2
27	0.07	0.51385	65	3	0.1875	48.330918	13.613803	47.4	6197.8	417.4	15.87	205	144	615	4.74	3.78
28	0.065	0.5124	65	3	0.1875	51.190417	13.23949	50.2	7408.6	528.5	14.68	194	134	582	7.60	6.58
29	0.06	0.5105	65	3	0.1875	56.339749	12.890317	55.2	9062.6	711.5	13.48	184	124	552	12.75	11.62
30	0.055	0.5079	65	3	0.1875	66.259018	12.532297	64.9	11337.5	1046.8	12.27	174	114	522	22.67	21.34
31	0.055	0.50855	65	4	0.1875	56.070386	14.472143	54.9	11307.8	883.5	12.29	174	114	696	12.48	11.36
32	0.06	0.511	65	4	0.1875	50.669012	14.885534	49.7	9045.7	638.7	13.49	184	124	736	7.08	6.07

Table E - 2

AIR CURTAIN DESIGN	Created: Warren T. Jones, Ph.D.	10/29/08 11:05 AM
Solutions Summary	Last Revision: 12/19/08 9:42 AM	

Solution #	Max Speed of Sound Ratio c/c _w (-)	Non-Dim Height, z/H, at Max c/c _w (-)	Depth of Manifold [H] (ft)	Number of nozzles per ft [n] (1/ft)	Diameter of nozzle exit [d] (in)	Manifold Pressure [Pm] (psia)	Diameter of manifold [Dman] (in)	Pressure at Manifold End [Pend] (psia)	Flow Rate (scfm)	Total Pneumatic HP at manifold (hp)	Rise Time (sec)	Manifold length (ft)	Manifold Position in front of array (ft)	Total Number of Nozzles (-)	Pressure Diff at Manifold Beginning (psi)	Pressure Diff at Manifold End (psi)
33	0.065	0.51275	65	4	0.1875	47.829587	15.327987	46.9	7436.5	495.7	14.69	195	134	780	4.24	3.28
34	0.0689038	0.51385	65	4	0.1875	46.519274	15.604227	45.6	6410.6	415.6	15.61	202	142	808	2.93	2.00
35	0.0981816	0.51735	65	3	0.125	46.519274	10.26494	45.6	2761.0	179.0	22.53	261	200	783	2.93	2.00
36	0.09	0.5165	65	3	0.125	48.630176	9.9155285	47.7	3379.6	229.0	20.59	244	184	732	5.04	4.07
37	0.08	0.515	65	3	0.125	54.178391	9.4911297	53.1	4476.4	338.0	18.22	224	164	672	10.59	9.51
38	0.07	0.51255	65	3	0.125	68.653791	9.0504359	67.3	6200.3	593.2	15.84	204	144	612	25.06	23.69
39	0.065	0.5107	65	3	0.125	84.64842	8.8231482	83.0	7460.1	880.0	14.64	194	134	582	41.06	39.37
40	0.06	0.5082	65	3	0.125	109.444	8.5908675	107.3	9148.2	1395.2	13.43	184	123	552	65.86	63.67
41	0.0894442	0.5167	65	4	0.125	46.519274	11.426768	45.6	3427.4	222.2	20.47	243	183	972	2.93	2.00
42	0.08	0.51535	65	4	0.125	49.482031	10.961129	48.5	4469.6	308.2	18.23	224	164	896	5.89	4.90
43	0.07	0.51315	65	4	0.125	57.372836	10.452303	56.2	5185.5	494.5	15.85	204	144	816	13.78	12.64
44	0.065	0.5115	65	4	0.125	65.921808	10.189684	64.6	7436.8	683.2	14.65	194	134	776	22.33	21.01
45	0.06	0.50925	65	4	0.125	81.738902	9.9209885	80.1	9109.3	1037.6	13.45	184	124	736	38.15	36.52
46	0.0713653	0.52915	60	3	0.1875	44.251701	13.586476	43.4	4693.0	304.9	15.83	204	144	612	2.89	2.00
47	0.07	0.5288	60	3	0.1875	44.624658	13.484736	43.7	4912.2	321.9	15.51	201	141	603	3.26	2.37
48	0.06	0.5257	60	3	0.1875	50.064817	12.822704	49.1	7233.5	531.8	13.19	182	121	546	8.70	7.70
49	0.055	0.5233	60	3	0.1875	56.719095	12.461978	55.6	9030.7	752.1	12.01	172	111	516	15.35	14.22
50	0.05	0.5198	60	3	0.1875	70.535281	12.091499	69.1	11592.1	1200.6	10.83	162	101	486	29.17	27.76
51	0.0650933	0.5278	60	4	0.1875	44.251701	15.213664	43.4	5889.2	382.7	14.38	192	131	768	2.89	2.00
52	0.06	0.5261	60	4	0.1875	46.212217	14.807441	45.3	7222.5	490.1	13.19	182	121	728	4.85	3.92
53	0.05	0.5206	60	4	0.1875	57.322759	13.963146	56.2	11555.8	972.7	10.84	162	102	648	15.96	14.81
54	0.045	0.5158	60	4	0.1875	74.27812	13.522798	72.8	15359.1	1675.2	9.65	152	91	608	32.91	31.43
55	0.0927166	0.5317	60	3	0.125	44.251701	9.9667411	43.4	2515.2	163.4	20.75	246	185	738	2.89	2.00
56	0.09	0.5314	60	3	0.125	44.838417	9.8408507	43.9	2690.5	177.1	20.12	240	180	720	3.47	2.57
57	0.08	0.52995	60	3	0.125	48.629278	9.4320566	47.7	3571.6	255.0	17.81	221	160	663	7.26	6.29
58	0.07	0.5277	60	3	0.125	58.402125	8.9865335	57.2	4933.8	423.1	15.49	201	141	603	17.04	15.87
59	0.065	0.52605	60	3	0.125	69.057919	8.7567579	67.7	5925.5	600.9	14.32	191	131	573	27.69	26.31
60	0.06	0.52375	60	3	0.125	88.163899	8.5218236	86.4	7249.3	938.5	13.14	181	121	543	46.80	45.03
61	0.055	0.52055	60	3	0.125	116.83166	8.2813779	114.5	9075.7	1557.0	11.95	171	111	513	75.46	73.13
62	0.0844688	0.53095	60	4	0.125	44.251701	11.117868	43.4	3135.5	203.7	18.85	230	169	920	2.89	2.00
63	0.08	0.5303	60	4	0.125	45.418964	10.892861	44.5	3567.0	237.9	17.82	221	160	884	4.05	3.14
64	0.07	0.5282	60	4	0.125	50.788774	10.378594	49.8	4924.0	367.2	15.50	201	141	804	9.42	8.41
65	0.06	0.52465	60	4	0.125	67.065129	9.8687927	65.7	7264.0	715.3	13.16	182	121	728	25.70	24.36
66	0.055	0.5218	60	4	0.125	87.195912	9.5913291	85.5	9084.2	1163.1	11.98	172	111	688	45.83	44.09
67	0.0741161	0.5296	60	6	0.125	44.251701	12.99912	43.4	4294.2	279.0	16.46	210	149	1260	2.89	2.00
68	0.07	0.5287	60	6	0.125	45.499924	12.713148	44.6	4914.3	328.3	15.51	201	141	1206	4.13	3.22
69	0.06	0.5255	60	6	0.125	52.43698	12.088894	51.4	7239.0	557.4	13.18	182	121	1092	11.07	10.02
70	0.05	0.5194	60	6	0.125	78.882021	11.399569	77.3	11610.4	1344.8	10.82	162	101	972	37.52	35.94
71	0.0612811	0.5443	55	4	0.1875	41.989174	14.772019	41.1	5362.2	349.4	13.14	181	121	724	2.84	2.00
72	0.06	0.54385	55	4	0.1875	42.397929	14.688806	41.5	5669.1	373.0	12.85	179	119	716	3.25	2.41

Table E - 3

AIR CURTAIN DESIGN	Created: Warren T. Jones, Ph.D.	10/29/08 11:05 AM
Solutions Summary	Last Revision:	12/19/08 9:42 AM

Solution #	Max Speed of Sound Ratio c/c_w (-)	Non-Dim Height, z/H , at Max c/c_w (-)	Depth of Manifold [H] (ft)	Number of nozzles per ft [n] (1/ft)	Diameter of nozzle exit [d] (in)	Manifold Pressure [Pm] (psia)	Diameter of manifold [Dman] (in)	Pressure at Manifold End [Pend] (psia)	Flow Rate (scfm)	Total Pneumatic HP at manifold (hp)	Rise Time (sec)	Manifold length (ft)	Manifold Position in front of array (ft)	Total Number of Nozzles (-)	Pressure Diff at Manifold Beginning (psi)	Pressure Diff at Manifold End (psi)
73	0.05	0.5387	55	4	0.1875	49.735396	13.878792	48.7	9081.8	700.9	10.58	160	99	640	10.59	9.60
74	0.045	0.53425	55	4	0.1875	60.69544	13.434915	59.5	12028.2	1132.9	9.42	150	90	600	21.55	20.34
75	0.04	0.52725	55	4	0.1875	87.555772	12.977102	85.8	16705.5	2269.7	8.24	140	80	560	48.41	46.66
76	0.0872689	0.5486	55	3	0.125	41.984127	9.6592836	41.1	2279.2	148.5	18.97	231	170	693	2.84	2.00
77	0.08	0.5476	55	3	0.125	44.032604	9.352379	43.2	2803.8	191.6	17.34	217	156	651	4.89	4.01
78	0.07	0.5455	55	3	0.125	50.52671	8.9230567	49.5	3880.9	304.3	15.09	198	137	594	11.38	10.37
79	0.06	0.54185	55	3	0.125	70.360592	8.4765726	69.0	5711.5	623.6	12.81	179	118	537	31.22	29.81
80	0.055	0.53895	55	3	0.125	92.893603	8.2339115	91.0	7131.8	1028.0	11.67	169	109	507	53.75	51.89
81	0.0795106	0.5478	55	4	0.125	41.984127	10.77518	41.1	2841.5	185.1	17.24	216	156	864	2.84	2.00
82	0.07	0.5459	55	4	0.125	45.467914	10.305313	44.6	3874.6	273.4	15.09	198	137	792	6.32	5.41
83	0.06	0.5426	55	4	0.125	56.187687	9.7896677	55.1	5695.5	496.6	12.83	179	118	716	17.04	15.92
84	0.055	0.54	55	4	0.125	69.577496	9.5090102	68.2	7103.8	767.0	11.69	169	109	676	30.43	29.04
85	0.05	0.5362	55	4	0.125	94.603972	9.2210876	92.7	9111.1	1337.5	10.53	159	99	636	55.46	53.57
86	0.045	0.5552	50	3	0.1875	62.260706	11.557789	61.0	9331.0	955.7	9.14	148	87	444	25.34	24.09
87	0.05	0.5596	50	3	0.1875	49.354617	11.907556	48.4	7016.5	569.7	10.26	157	97	471	12.43	11.45
88	0.06	0.5647	50	3	0.1875	40.742539	12.617456	39.9	4396.4	294.7	12.46	176	115	528	3.82	3.01
89	0.0630358	0.5657	50	3	0.1875	39.716553	12.799138	38.9	3870.7	252.9	13.12	181	121	543	2.79	2.00
90	0.0575204	0.56405	50	4	0.1875	39.716553	14.358813	38.9	4875.8	318.6	11.92	171	111	684	2.79	2.00
91	0.05	0.56015	50	4	0.1875	43.81422	13.750859	42.9	7002.6	504.7	10.27	157	97	628	6.89	6.02
92	0.045	0.55605	50	4	0.1875	50.792549	13.346952	49.8	9302.5	777.3	9.15	148	87	592	13.87	12.85
93	0.04	0.54965	50	4	0.1875	68.365575	12.885146	67.0	12853.7	1445.7	8.02	138	78	552	31.44	30.08
94	0.08	0.56865	50	3	0.125	40.142457	9.2519218	39.3	2162.2	142.8	16.80	212	152	636	3.22	2.42
95	0.075	0.5678	50	3	0.125	41.745418	9.0464459	40.9	2529.9	173.7	15.72	203	143	609	4.82	3.99
96	0.07	0.5667	50	3	0.125	44.376572	8.837555	43.5	2998.0	218.9	14.63	194	134	582	7.45	6.57
97	0.065	0.56525	50	3	0.125	48.889171	8.6248812	47.9	3606.8	290.1	13.53	185	124	555	11.97	10.99
98	0.06	0.56335	50	3	0.125	57.07104	8.4080712	55.9	4418.5	414.8	12.43	176	115	528	20.15	19.01
99	0.055	0.5607	50	3	0.125	72.95887	8.1622474	71.5	5501.9	660.4	11.33	166	106	498	36.04	34.58
100	0.05	0.55685	50	3	0.125	99.374244	7.9356371	97.4	7087.6	1158.7	10.21	157	96	471	62.45	60.46
101	0.074572	0.568	50	4	0.125	39.716553	10.421174	38.9	2559.9	167.3	15.63	202	142	808	2.79	2.00
102	0.07	0.56705	50	4	0.125	41.077618	10.206535	40.3	2994.1	202.3	14.63	194	134	776	4.16	3.33
103	0.06	0.56395	50	4	0.125	48.015269	9.7107367	47.1	4408.5	348.2	12.45	176	115	704	11.09	10.13
104	0.055	0.56155	50	4	0.125	56.533788	9.4266659	55.4	5484.7	510.1	11.34	166	106	664	19.61	18.48
105	0.05	0.5581	50	4	0.125	74.191358	9.1643398	72.7	7055.3	861.1	10.23	157	96	628	37.27	35.79
106	0.0589005	0.5901	45	3	0.1875	37.44898	12.404913	36.7	3495.2	229.1	11.78	170	109	510	2.75	2.00
107	0.05	0.5857	45	3	0.1875	42.571107	11.796489	41.7	5329.5	397.2	9.90	154	75	408	7.87	7.02
108	0.04	0.57525	45	3	0.1875	70.44672	11.078176	69.0	9792.8	1207.6	7.74	136	75	408	35.75	34.34
109	0.0537618	0.5882	45	4	0.1875	37.44898	13.933313	36.7	4413.5	289.3	10.70	161	100	644	2.75	2.00
110	0.05	0.58615	45	4	0.1875	39.082228	13.622592	38.3	5321.2	364.0	9.90	154	94	616	4.38	3.60
111	0.04	0.5764	45	4	0.1875	54.162768	12.793059	53.1	9754.3	924.8	7.75	136	75	544	19.46	18.38
112	0.0375	0.5721	45	4	0.1875	65.495485	12.554166	64.2	11693.0	1340.6	7.20	131	71	524	30.80	29.49

Table E - 4

AIR CURTAIN DESIGN	Created: Warren T. Jones, Ph.D.	10/29/08 11:05 AM
Solutions Summary	Last Revision:	12/19/08 9:42 AM

Solution #	Max Speed of Sound Ratio c/c_w (-)	Non-Dim Height, z/H , at Max c/c_w (-)	Depth of Manifold [H] (ft)	Number of nozzles per ft [n] (1/ft)	Diameter of nozzle exit [d] (in)	Manifold Pressure [Pm] (psia)	Diameter of manifold [Dman] (in)	Pressure at Manifold End [Pend] (psia)	Flow Rate (scfm)	Total Pneumatic HP at manifold (hp)	Rise Time (sec)	Manifold length (ft)	Manifold Position in front of array (ft)	Total Number of Nozzles (-)	Pressure Diff at Manifold Beginning (psi)	Pressure Diff at Manifold End (psi)
113	0.035	0.5664	45	4	0.1875	83.210117	12.359883	81.5	14402.1	2097.8	6.64	127	66	508	48.51	46.85
114	0.0764369	0.5937	45	3	0.125	37.44898	9.0127348	36.7	1836.7	120.4	15.44	201	140	603	2.75	2.00
115	0.07	0.59245	45	3	0.125	39.469314	8.7527704	38.7	2282.1	157.7	14.09	190	129	570	4.77	3.98
116	0.06	0.58935	45	3	0.125	47.444082	8.3159294	46.5	3349.7	278.2	11.99	172	111	516	12.74	11.80
117	0.05	0.58345	45	3	0.125	76.781633	7.8609573	75.2	5371.6	722.0	9.86	154	93	462	42.08	40.55
118	0.045	0.5782	45	3	0.125	108.50122	7.6257986	106.3	7147.1	1357.4	8.78	145	84	435	73.80	71.63
119	0.0696558	0.59265	45	4	0.125	37.44898	10.08135	36.7	2302.7	151.0	14.03	189	128	756	2.75	2.00
120	0.06	0.58985	45	4	0.125	41.760923	9.6044154	40.9	3343.7	244.4	12.00	172	111	688	7.06	6.23
121	0.05	0.5845	45	4	0.125	58.010362	9.0786138	56.9	5352.5	543.5	9.88	154	93	616	23.31	22.15
122	0.045	0.57975	45	4	0.125	80.930775	8.8063192	79.3	7108.0	1007.0	8.80	145	84	580	46.23	44.61
123	0.04	0.60835	40	3	0.1875	53.994182	10.957167	52.9	7252.8	732.4	7.43	133	73	399	21.52	20.44
124	0.045	0.6142	40	3	0.1875	42.149864	11.326312	41.3	5257.0	414.4	8.46	142	81	426	9.67	8.83
125	0.05	0.618	40	3	0.1875	37.333925	11.685474	36.6	3981.9	278.0	9.47	151	90	453	4.86	4.11
126	0.0547881	0.62055	40	3	0.1875	35.181406	11.997706	34.5	3136.0	206.3	10.44	159	98	477	2.70	2.00
127	0.036	0.6024	40	4	0.1875	57.105438	12.31295	56.0	9770.7	1043.5	6.60	126	66	504	24.63	23.49
128	0.038	0.6062	40	4	0.1875	49.266343	12.508325	48.3	8390.4	773.1	7.02	130	69	520	16.79	15.80
129	0.04	0.60925	40	4	0.1875	44.266045	12.653509	43.4	7231.2	598.7	7.44	133	73	532	11.79	10.90
130	0.045	0.61475	40	4	0.1875	37.847879	13.079771	37.1	5247.4	371.4	8.46	142	81	568	5.37	4.61
131	0.047	0.6164	40	4	0.1875	36.521234	13.219603	35.8	4656.3	318.0	8.87	145	85	580	4.04	3.31
132	0.048	0.6171	40	4	0.1875	36.005634	13.311729	35.3	4411.8	297.1	9.07	147	87	588	3.53	2.81
133	0.0710592	0.6247	40	3	0.125	35.181406	8.6712722	34.5	1630.4	107.3	13.69	186	126	558	2.70	2.00
134	0.07	0.6245	40	3	0.125	35.447497	8.6226153	34.7	1689.9	112.0	13.47	184	124	552	2.97	2.26
135	0.065	0.62325	40	3	0.125	37.207997	8.4248908	36.5	2036.1	141.7	12.47	176	115	528	4.73	3.99
136	0.06	0.6216	40	3	0.125	40.342035	8.1996444	39.5	2482.6	187.3	11.47	167	107	501	7.86	7.06
137	0.055	0.61935	40	3	0.125	46.277932	7.9949465	45.4	3111.1	269.3	10.46	159	98	477	13.80	12.87
138	0.05	0.6162	40	3	0.125	58.495094	7.7606967	57.3	3979.6	435.4	9.45	150	90	450	26.02	24.85
139	0.045	0.61145	40	3	0.125	82.248153	7.5477458	80.6	5305.7	816.1	8.42	142	81	426	49.77	48.13
140	0.064765	0.6235	40	4	0.125	35.181406	9.7019234	34.5	2045.4	134.6	12.43	175	115	700	2.70	2.00
141	0.06	0.622	40	4	0.125	36.855422	9.470115	36.1	2479.1	170.9	11.48	167	107	668	4.38	3.64
142	0.05	0.617	40	4	0.125	46.683403	8.9632239	45.7	3968.7	346.5	9.46	150	90	600	14.21	13.27
143	0.045	0.6127	40	4	0.125	61.429316	8.7166705	60.2	5283.6	607.0	8.44	142	81	568	28.95	27.72
144	0.04	0.60585	40	4	0.125	90.781357	8.4332861	89.0	7313.3	1241.7	7.40	133	72	532	58.30	56.49
145	0.035	0.6412	35	3	0.1875	62.13753	10.492844	60.9	7748.6	966.6	6.06	122	61	366	31.88	30.64
146	0.0375	0.64635	35	3	0.1875	49.867873	10.665372	48.9	6334.6	634.2	6.56	126	65	378	19.61	18.61
147	0.04	0.65025	35	3	0.1875	42.82438	10.835685	42.0	5273.6	453.4	7.05	130	70	390	12.57	11.71
148	0.045	0.6557	35	3	0.1875	35.99639	11.169978	35.3	3813.5	275.6	8.02	138	78	414	5.74	5.02
149	0.05	0.65925	35	3	0.1875	33.16137	11.49652	32.5	2880.0	191.7	8.97	146	86	438	2.91	2.24
150	0.0657119	0.66455	35	3	0.125	32.913832	8.3156937	32.3	1434.3	94.8	11.94	171	111	513	2.66	2.00
151	0.06	0.6628	35	3	0.125	34.96675	8.0835878	34.3	1804.6	126.7	10.86	162	102	486	4.71	4.01
152	0.055	0.66075	35	3	0.125	38.463577	7.8738928	37.7	2255.1	174.1	9.91	154	94	462	8.21	7.44

Table E - 5

AIR CURTAIN DESIGN	Created: Warren T. Jones, Ph.D.	10/29/08 11:05 AM
Solutions Summary	Last Revision: 12/19/08 9:42 AM	

Solution #	Max Speed of Sound Ratio c/c _w (-)	Non-Dim Height, z/H, at Max c/c _w (-)	Depth of Manifold [H] (ft)	Number of nozzles per ft [n] (1/ft)	Diameter of nozzle exit [d] (in)	Manifold Pressure [Pm] (psia)	Diameter of manifold [Dman] (in)	Pressure at Manifold End [Pend] (psia)	Flow Rate (scfm)	Total Pneumatic HP at manifold (hp)	Rise Time (sec)	Manifold length (ft)	Manifold Position in front of array (ft)	Total Number of Nozzles (-)	Pressure Diff at Manifold Beginning (psi)	Pressure Diff at Manifold End (psi)
153	0.05	0.6578	35	3	0.125	45.534518	7.6604183	44.6	2893.3	264.5	8.96	146	86	438	15.28	14.37
154	0.045	0.6535	35	3	0.125	61.252839	7.442843	60.0	3840.0	472.2	7.99	138	77	414	31.00	29.77
155	0.0425	0.6505	35	3	0.125	73.849235	7.3325391	72.4	4495.5	666.5	7.50	134	73	402	43.59	42.12
156	0.04	0.64665	35	3	0.125	90.309053	7.2210861	88.5	5333.3	967.0	7.01	130	69	390	60.05	58.25
157	0.038	0.6427	35	3	0.125	107.37265	7.1084364	105.2	6145.9	1324.8	6.61	126	66	378	77.12	74.97
158	0.08	0.45215	100	3	0.1875	77.530347	14.749655	76.0	16592.5	1321.2	20.14	241	180	723	18.39	16.84
159	0.09	0.4541	100	3	0.1875	67.801897	15.412713	66.4	12497.9	870.3	22.80	263	203	789	8.66	7.30
160	0.1	0.45535	100	3	0.1875	63.604798	16.050135	62.3	9745.8	636.6	25.45	285	225	855	4.46	3.19
161	0.1052052	0.4558	100	3	0.1875	62.39229	16.388034	61.1	8672.8	555.7	26.82	297	237	891	3.25	2.00
162	0.07	0.4498	100	4	0.1875	83.402368	16.195516	81.7	22907.1	1962.1	17.49	218	158	872	24.26	22.59
163	0.08	0.4526	100	4	0.1875	69.345256	17.032353	68.0	16559.7	1179.4	20.16	241	180	964	10.20	8.81
164	0.09	0.45435	100	4	0.1875	63.979295	17.797875	62.7	12481.7	820.1	22.81	263	203	1052	4.83	3.56
165	0.0958903	0.4551	100	4	0.1875	62.39229	18.236028	61.1	10746.1	688.6	24.37	276	216	1104	3.25	2.00
166	0.1	0.45435	100	3	0.125	82.451387	10.697362	80.8	9790.3	829.0	25.41	285	225	855	23.31	21.66
167	0.11	0.45545	100	3	0.125	71.838043	11.125752	70.4	7857.6	579.7	28.06	308	247	924	12.69	11.26
168	0.12	0.4563	100	3	0.125	66.484545	11.522485	65.2	6422.6	438.5	30.72	330	269	990	7.34	6.01
169	0.13	0.45685	100	3	0.125	63.593894	11.907819	62.3	5343.2	349.0	33.37	352	292	1056	4.45	3.18
170	0.1367309	0.4572	100	3	0.125	62.39229	12.164634	61.1	4763.1	305.2	35.16	367	307	1101	3.25	2.00
171	0.08	0.451	100	4	0.125	114.29008	11.329055	112.0	16614.3	1950.1	20.10	240	180	960	55.15	52.86
172	0.09	0.4533	100	4	0.125	84.472198	11.862948	82.8	12542.6	1088.1	22.77	263	202	1052	25.33	23.64
173	0.1	0.4548	100	4	0.125	72.040292	12.353781	70.6	9770.2	722.9	25.43	285	225	1140	12.90	11.46
174	0.11	0.4558	100	4	0.125	66.214844	12.84836	64.9	7845.7	533.5	28.08	308	247	1232	7.07	5.75
175	0.1245854	0.4568	100	4	0.125	62.39229	13.510036	61.1	5883.5	377.0	31.94	340	280	1360	3.25	2.00
176	0.15	0.39905	200	3	0.1875	122.50531	19.746064	120.1	40107.6	2881.1	42.82	432	372	1296	18.92	16.47
177	0.175	0.4002	200	3	0.1875	110.7052	21.164454	108.5	28359.6	1841.0	50.34	496	435	1488	7.12	4.90
178	0.18	0.40035	200	3	0.1875	109.54388	21.420424	107.4	26580.9	1707.4	51.85	508	448	1524	5.95	3.76
179	0.19	0.4006	200	3	0.1875	107.81894	21.965031	105.7	23563.4	1489.7	54.89	534	474	1602	4.23	2.07
180	0.1905391	0.40065	200	3	0.1875	107.74376	21.985775	105.6	23397.4	1478.2	55.05	535	475	1605	4.15	2.00
181	0.15	0.39935	200	4	0.1875	114.13595	22.801421	111.9	40046.5	2680.2	42.84	432	372	1728	10.55	8.26
182	0.16	0.3998	200	4	0.1875	110.60441	23.480005	108.4	34668.9	2248.5	45.84	458	397	1832	7.02	4.80
183	0.17	0.4002	200	4	0.1875	108.37533	24.115153	106.2	30222.7	1920.6	48.85	483	423	1932	4.79	2.62
184	0.1738586	0.40035	200	4	0.1875	107.74376	24.364709	105.6	28747.5	1816.2	50.01	493	432	1972	4.15	2.00
185	0.13	0.39495	200	3	0.125	325.08378	12.342891	318.6	56118.2	10697.3	36.64	380	319	1140	221.49	214.99
186	0.15	0.39755	200	3	0.125	205.94944	13.14681	201.8	40323.9	4869.6	42.70	431	371	1293	102.36	98.24
187	0.175	0.3993	200	3	0.125	140.70459	14.093382	137.9	28433.6	2345.9	50.27	495	435	1485	37.12	34.30
188	0.2	0.40025	200	3	0.125	119.29639	14.982992	116.9	21041.9	1471.9	57.89	559	499	1677	15.71	13.32
189	0.225	0.40085	200	3	0.125	110.96905	15.83846	108.7	16146.8	1050.7	65.60	624	564	1872	7.38	5.16
190	0.2459976	0.4012	200	3	0.125	107.74376	16.542811	105.6	13217.2	835.0	72.17	680	619	2040	4.15	2.00

Table E - 6

AIR CURTAIN DESIGN	Created: Warren T. Jones, Ph.D.	10/29/08 11:05 AM
Solutions Summary	Last Revision:	12/19/08 9:42 AM

Solution #	Max Speed of Sound Ratio c/c_w (-)	Non-Dim Height, z/H , at Max c/c_w (-)	Depth of Manifold [H] (ft)	Number of nozzles per ft [n] (1/ft)	Diameter of nozzle exit [d] (in)	Manifold Pressure [Pm] (psia)	Diameter of manifold [Dman] (in)	Pressure at Manifold End [Pend] (psia)	Flow Rate (scfm)	Total Pneumatic HP at manifold (hp)	Rise Time (sec)	Manifold length (ft)	Manifold Position in front of array (ft)	Total Number of Nozzles (-)	Pressure Diff at Manifold Beginning (psi)	Pressure Diff at Manifold End (psi)
191	0.15	0.39825	200	4	0.125	159.2735	15.199215	156.1	40277.1	3761.6	42.76	432	371	1728	55.68	52.50
192	0.175	0.3997	200	4	0.125	124.14648	16.274781	121.7	28374.3	2065.5	50.30	495	435	1980	20.56	18.07
193	0.18	0.3999	200	4	0.125	120.75809	16.488306	118.3	26642.8	1886.6	51.82	508	448	2032	17.17	14.75
194	0.19	0.40025	200	4	0.125	115.74869	16.907642	113.4	23610.0	1602.5	54.86	534	473	2136	12.16	9.84
195	0.2	0.40055	200	4	0.125	112.35767	17.317358	110.1	21050.2	1386.9	57.91	560	499	2240	8.77	6.52
196	0.21	0.40075	200	4	0.125	110.0131	17.703056	107.8	18837.2	1215.2	60.98	585	525	2340	6.42	4.22
197	0.22	0.40095	200	4	0.125	108.36182	18.110765	106.2	16995.9	1079.9	64.06	612	551	2448	4.77	2.61
198	0.2248209	0.40105	200	4	0.125	107.74376	18.289433	105.6	16171.7	1021.7	65.56	624	564	2496	4.15	2.00

